The relation between dynamics and activity of phospholipase A/acyltransferase homologs

Chatterjee, S.D.

2

Chapter

Sub-second ^{15}N backbone dynamics reveal differences between PLAAT3 and PLAAT4.

The work in this chapter was published as: Chatterjee, S. D., Zhou, J., Dasgupta, R., Cramer-Blok, A., Timmer, M., van der Stelt, M., and Ubbink, M. (2021) Protein Dynamics Influence the Enzymatic Activity of Phospholipase A/Acyltransferases 3 and 4. Biochemistry 60, 1178–1190.

Abstract

PLAAT3 and PLAAT4, despite being homologs, clearly differ in substrate specificity, activity and physiological roles. The effect of the amino acid differences on protein dynamics between the two enzymes were studied. Thermostability experiments revealed that PLAAT3 is inherently more thermostable than PLAAT4 owing to a well dispersed mesh of salt bridges. Despite having similar molecular weights, τ_c was observed to be higher for PLAAT4 owing to an elongated structure. Fast timescale NMR dynamics confirmed the presence of a highly disordered loop in both enzymes while PLAAT3 was observed to be quite non-flexible otherwise. Globally, PLAAT4 was found to be more dynamic and low order parameters were observed in the active site region indicating a dynamic active site. Slow timescale dynamics also confirmed a presence of a dynamic active site in PLAAT4, absent in PLAAT3.

Introduction

Phospholipases A/acyltransferases (PLAATs) are a family of enzymes that are sequentially homologous and structurally similar to lecithin:retinol acyltransferase (LRAT).[1] Due to its resemblance to LRAT, they are also part of the bigger eukaryotic superfamily of NlpC/P60.[2] They were identified as enzymes due to their similarities in structure with LRAT.[2] In human tissues, the genes of five members of the PLAATs are expressed and the enzymes are named as PLAAT1 to PLAAT5, although many other names exist in the literature. The enzymes were originally discovered as class II tumor suppressors[3–5] and were named as HRAS-like suppressor (HRASLS).[6,7] HRASLS genes are ubiquitously expressed in most normal tissues, but downregulated in most types of tumor cells.[8] The relationship between the tumor suppressor function and acyltransferase activity remains unclear.[9]

In the past several years, it was reported that all five members possess phospholipase A1/A2 activity (hydrolysis of the *sn-1* or *sn-2* ester bonds of PtdCho or PtdEt) and N-acyl phosphatidylethanolamines (NAPE)-forming N-acyltransferase activity, which releases an acyl group from the *sn-1* or *sn-2* position of phosphatidylcholine (PtdCho) and/or transfers it to phosphatidylethanolamine (PtdEt) in

a Ca^{2+}-independent manner, see Figure 2.1C.[10] These enzymes also have O-acyltransferase (AT) activity (transfer of an acyl group from PtdCho to the hydroxyl group of lyso PtdCho.[1,6,7] PLAAT3 and PLAAT4 both contain the N-terminal NlpC/P60 domain and have conserved sequences, showing 58% identity and 72% similarity (Figure 2.1A). They have the characteristic NCEHFV motif of PLAATs, in which C represents C113, the nucleophile that forms a catalytic triad with two histidine residues. H23 acts as a base and H35 as the stabilizer (Figure 2.1D). [1,2,7] Xiaobai *et al.* have previously determined the solution structure (PDB: 2KYT) of the N-terminal domain (NTD) of PLAAT3 (PLAAT3N, residues 1–125),[11] revealing that PLAAT3N adopts a fold highly similar to those of the NlpC/P60 peptidase domains (Figure 2.1B).The same group also reported the solution structure of the NTD of PLAAT4 (PLAAT4N, residues 1–125, PDB ID: 2MY9).[12] The crystal structure of the NTD of PLAAT3 has been reported by Golczack *et al*. (PDB ID: 4DPZ) with a similar fold to that of the NMR structure (RMSD 0.74 for the Cα atoms of the non-flexible residues). The flexible loop and a few other residues could not be observed due to disorder.[1]

The two proteins comprise of six β strands and three (PLAAT3) or four (PLAAT4) α helices and one large loop (residues 38-57) that connects two β strands. We introduce minor modifications to the naming conventions of the secondary structural elements published in [11,12], see Table 2.1, Figure 2.2). We have included the nomenclature for two main loops L1 (residues 38-57) and L2 (residue 100-109/110) and the β strand B6 (residues 103-104) as a part of the loop L2 and thus renamed as L2(B6).

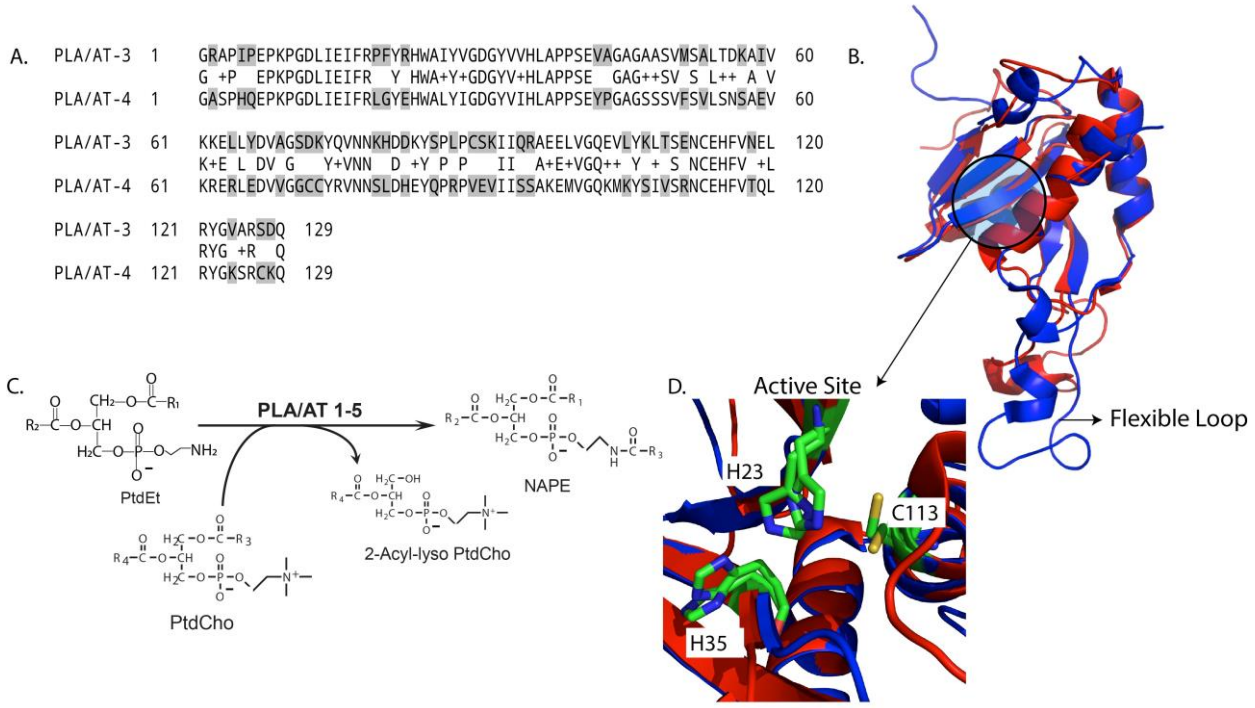

Figure 2.1 Sequence and structural comparisons between PLAAT3 and PLAAT4. (A) Sequence alignment performed by protein-protein BLAST (blastp).[31] Residues highlighted in gray are variable residues and '+' symbols represent conservative substitutions. The proteins share 58% sequence identity and 72% similarity. (B) Superposition of the PLAAT3 (red, PDB ID: 2KYT,[11]) and PLAAT4 (blue, PDB ID: 2MY9, [12]) structures. The rmsd is 0.78 Å for the Cα positions in non-flexible residues (PLAAT3: 9-36, 63-124 and PLAAT4: 9-35, 54-124). (C) The N-acyltransferase reaction catalyzed by PLAATs. PdEt: phosphatidylethanolamine, NAPE: N-acylphosphatidylethanolamine, PtdCho: phosphatidylcholine, 2-Acyl-lyso PtdCho: 2-Acyl-lyso phospthatidylcholine. (D) Zoom of the active site with representative members of the catalytic triad. C113 acts as the nucleophile where H23 serves as the base and H35 stabilizes the charge on H23.

Table 2.1. Modified nomenclature of the secondary structural elements of PLAAT3 and PLAAT4. N: N-terminal residues, B: β-strand, L: loop, A: α-helix, C: C-terminal residues.

PLAAT3		**PLAAT4**	
Name	**Residues**	**Residues**	**Name**
N	1-12	N	1-10
B1	13-18	B1	13-17
B2	21-29	B2	23-29
B3	32-37	B3	32-37
L1	38-57	L1	38-57

B4	58-64	B4	58-64
A1	65-68	A1	65-69
B5	73-76	B5	73-76
A2	89-99	A2’	79-82
L2(B6)	100-109	A2	89-99
A3	110-122	L2(B6)	100-110
C	123-125	A3	112-122
		C	123-125

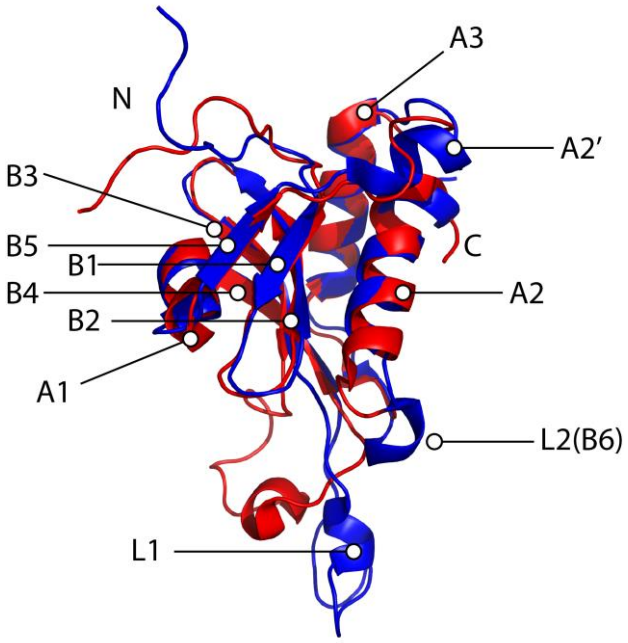

Figure 2.2 Modified nomenclature of PLAAT3 (red, PDB ID: 2KYT) and PLAAT4 (blue, PDB ID: 2MY9) according to Table 2.1.

Despite having similar amino acid sequences and structural homology, PLAAT3 and PLAAT4 differ greatly in activity. Uyama *et al.* reported a difference in phospholipase activity between full length PLAAT3 and PLAAT4 and stated that PLAAT3 has a maximal activity that is 4.8-fold larger than that of PLAAT4 in the mammalian cell homogenates.[13] This was confirmed by Pang *et al.* using full length MBP-PLAAT3 fusion proteins to assay the phospholipase activity with fluorescent BODIPY-labelled substrates dissolved in liposomes.[14] Interestingly, Golczak *et al.* showed the opposite in case of the soluble NTDs of these PLAATs, using short chain phosphatidylcholines as substrates and tracking the intermediates using mass spectrometry.[1] Clearly, despite the structural similarities, the activity depends both the on the exact sequence (PLAAT3 or -4) and the state (truncated – full length). Given the structural similarity between PLAAT3 and -4, we wondered whether differences in protein dynamics could explain the differences in activity. The dynamics of the soluble NTDs of PLAAT3 and PLAAT4 were studied using NMR spectroscopy on the fast, nanosecond, and slower, millisecond timescales. Such experiments are very demanding in terms of sample quality, size and stability, so we decided to work, at least initially, on the truncated N-terminal soluble part of the protein. From now onwards, any reference to PLAAT3 or PLAAT4 will therefore refer to the truncated versions of the proteins. The results show significant differences in dynamics in these two proteins, especially around the active site in PLAAT4.

Results

To characterize the differences in dynamics between PLAAT3 and PLAAT4, the melting temperature and the mobility of various timescales was determined. The N-terminal domains of PLAATs were expressed and purified by procedure mentioned in Materials and Methods.

Thermostability. A thermofluor-based assay was carried out to determine the melting temperatures (T_m) of PLAAT3 and PLAAT4 using the hydrophobic fluorescent probe SYPRO ORANGE. The T_m values were found to be 78.0 (±0.5) °C for PLAAT3 and 62.5 (±0.5) °C for PLAAT4. The large difference of 15 °C suggests that PLAAT3 has a more rigid structure with strong inter-residue, noncovalent interactions.

^{15}N-^{1}H HSQC spectra. NMR samples of PLAAT3 and PLAAT4 were prepared by producing ^{15}N-labelled proteins in *E. coli* BL21-DE3 pLys, with yields of around 40 mg/L. Concentrations of around 1.5 mM could be reached for NMR data acquisition. ^{15}N-^{1}H HSQC spectra of PLAAT3 and PLAAT4 were assigned based on the published data,[15,16] using the BMRB depositions (see Materials and Methods and Figure 2.3). Fewer resonances are observed in the spectrum of PLAAT4 than for that of PLAAT3, which suggests that more amides are mobile on the millisecond timescale or their protons in rapid exchange with the solvent, causing line broadening due to chemical exchange.

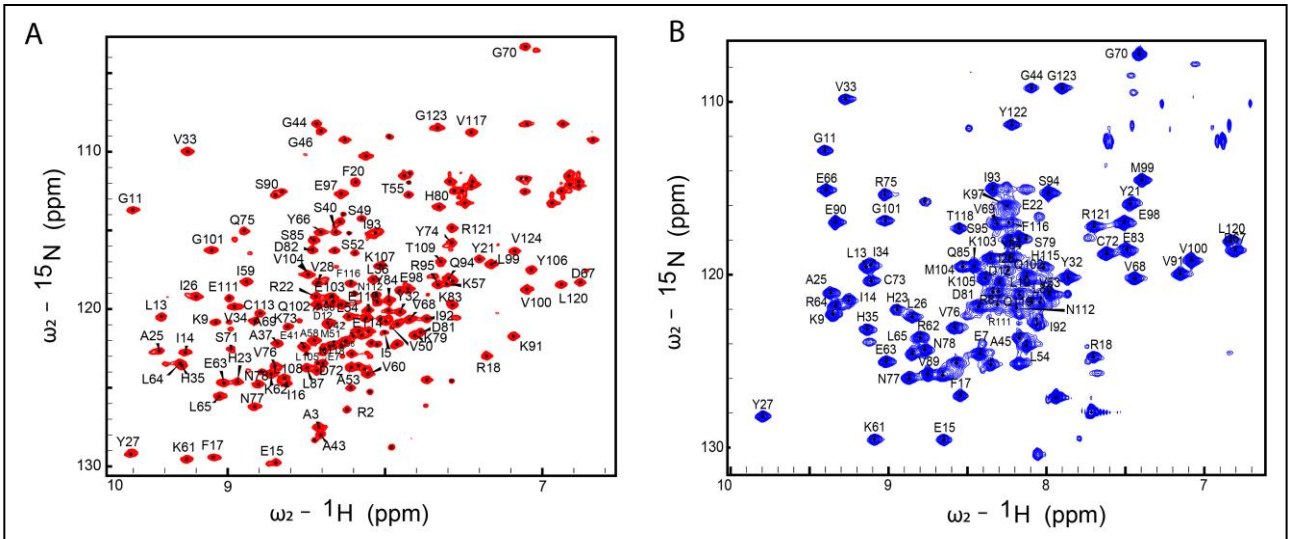

Figure 2.3 ^{15}N-^{1}H HSQC spectra of PLAAT3 (A) and PLAAT4 (B). NMR samples contained about 1.5 mM protein and 50 mM Tris, pH 7.5, 50 mM NaCl, 7% D_2O. Spectra were acquired at 25 °C at 14 T.

Fast motions. To determine the motions of PLAAT3 and PLAAT4 at pico-nanosecond timescale, the ^{15}N backbone amide T_1, T_2 and heteronuclear NOE parameters were determined at 14 T (600 MHz ^1H frequency) and 20 T (850 MHz). The data are presented in Figure 2.4 and Table S2.1(a-d). Relaxation parameters could be determined for 98 residues of PLAAT3 and 71 residues of PLAAT4. It is clear that the T_1/T_2 ratio is much larger for PLAAT4 than for PLAAT3, suggesting that the rotational correlation times differ, even though the two proteins have similar molecular weights. The low NOE values of L1 in both proteins indicate that this loop is highly disordered, which is in line with previous findings.[1,11,12] Due to the flexibility of the N-terminus and loop L1, the NOE and T_2 values of those regions differ much from the rigid parts of the proteins and should not be considered for the average T_1, average T_2 and average NOE calculations. Therefore, we calculated the 20% trimmed average values of T_1, T_2 and NOE, given in Table 2.2. Trimmed average NOE and T_1 values for PLAAT4 were higher than for PLAAT3 and T_2 values for PLAAT4 were lower.

To determine the rotational correlation times (τ_c) by Bruker Protein Dynamics software suite, three criteria were applied to exclude highly flexible residues. First, only residues with NOE values > 0.65 were included. Second, the T_1 value had to be within one standard deviation and, third, the T_2 is not much larger than the mean, $[(T_2-T_{2,mean})/T_2<3*(T_1-T_{1,mean})/T_1]$. The derived rotational correlation times are 8.4 ns and 12.5 ns for PLAAT3 and -4, respectively. This is remarkable, because both proteins have similar molecular weights, of 14.4 kDa and 14.7 kDa, respectively, and the NMR solutions and temperature were same for both proteins. Theoretical estimations of average τ_c from all models in the NMR ensemble structures (2kyt.pdb[11] for PLAAT3 and 2my9.pdb[12] for PLAAT4) using HYDRONMR[17] yield 9 ± 1 ns and 11 ± 1 ns, respectively, values close to experimentally determined ones. PLAAT3 is more globular with a compact structure, perhaps due to a distributed network of 17 salt bridges, whereas PLAAT4 is a more elongated molecule with only 10 salt bridges, concentrated in certain parts of the protein, as illustrated in Fig. 2.5. It can also not be excluded that PLAAT4 has a tendency for transient self-interactions under the high concentration (1.5 mM) used in the NMR samples, leading to a higher τ_c. Residues with NOE values below two standard deviation of the trimmed average were identified as residues showing internal motions and residues with T_1/T_2 ratios two standard deviation above or below the trimmed mean were identified as exhibiting additional motion. The residues demonstrating fast timescale dynamics are mapped on the structures of both proteins (Figure 2.6). Also, residues for which resonances are not found in the spectra are indicated, as these are likely to be involved in motions or exchange processes.

Table 2.2. 20% trimmed average and standard deviation in brackets of T_1, T_2 and NOE values of PLAAT3 and PLAAT4 obtained at 14 T (600 MHz) and 20 T (850 MHz) experiments. The rotational correlation ti1e τ_c for PLAAT3 was calculated using subsets of 40 (600 MHz) or 57 residues (850 MHz). For PLAAT4, τ_c subsets of 33 (600 MHz) and 37 residues (850 MHz) were used.

	600MHz			850 MHz		
PLAAT3	T_1 (ms)	T_2 (ms)	NOE	T_1 (ms)	T_2 (ms)	NOE
20% Trimmed Mean	720(2)	90(1)	0.66(0.01)	1060(5)	80(2)	0.78(0.02)
τ_c	8.5(0.2) ns			8.2(0.4) ns		
PLAAT4						
20% Trimmed Mean	900(4)	50(8)	0.71(0.01)	1380(10)	40(1)	0.83(0.01)
τ_c	12.6(0.3) ns			12.5(0.4) ns		

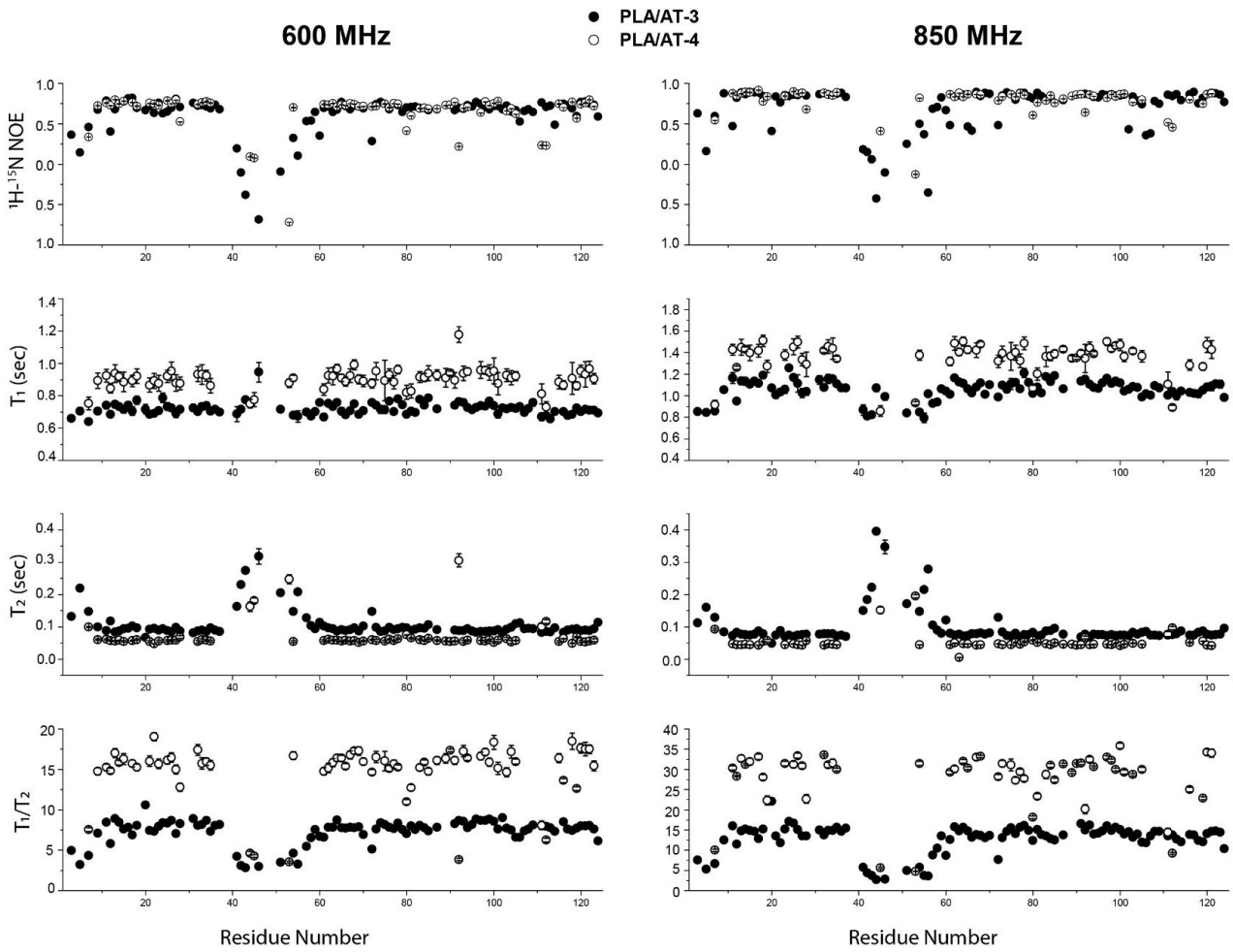

Figure 2.4 Relaxation data for PLAAT3 (solid circles) and PLAAT4 (open circles) at 14 T (600 MHz) and 20 T (850 MHz). The ^{15}N-NOE, ^{15}N-T_1, and ^{15}N-T_2 as well as T_1/T_2 are plotted against the residue number. Errors were estimated by the Monte Carlo method using 95% confidence level incorporated in Bruker Protein Dynamics software suite.

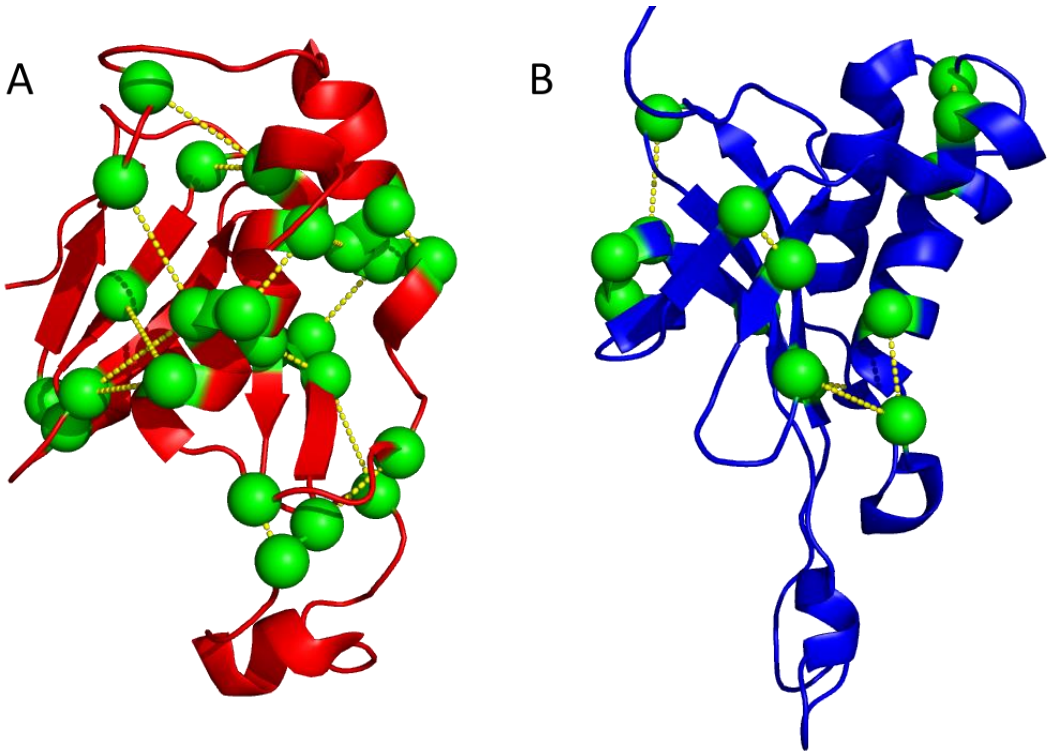

Figure 2.5 Representation of salt bridge networks (yellow dashes) in PLAAT3 (PDB ID: 2KYT) (A) and PLAAT4 (PDB ID: 2MY9) (B). Salt bridges were defined as a pair of basic and acidic residues with a nitrogen and an oxygen atom of the basic and acidic sidechains, respectively, within 3.2 Å in at least one of the 20 NMR structures. Green spheres represent the Cα atoms of the bridged residues.

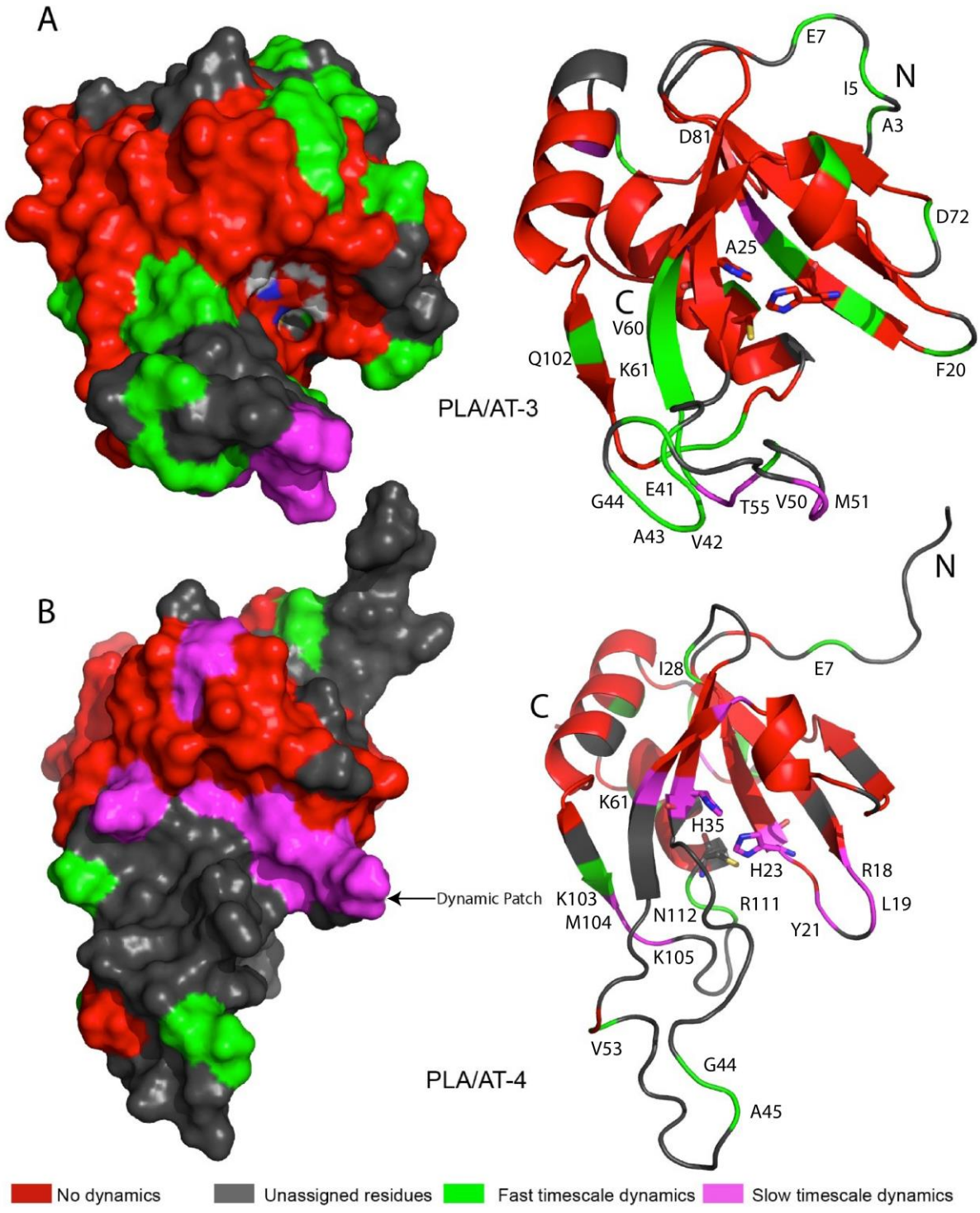

Figure 2.6 Dynamics profiles mapped on the structures of PLAAT3 (A), PDB ID: 2KYT,[11] and PLAAT4 (B), PDB ID: 2MY9.[12] Unassigned residues are shown in gray, residues showing neither fast nor slow-timescale motions are shown in red, residues showing only slow-timescale dynamics are in pink and residues showing only fast-timescale dynamics are shown in green. Residues in fast or slow-timescale motions are labelled. The dynamic patch present in PLAAT4 that includes the catalytic triad residues H23 and H35 is labelled.

The Lipari-Szabo model-free method [18,19] was used to derive the order parameters (S^2) of the backbone amides from the ^{15}N relaxation data. Only the model that allowed fitting of S^2 and the time constant of the fast dynamics (τ_e) was used, to avoid overfitting (see Materials and Methods). The order parameters are plotted in Figure 2.7 and the results are listed in Table S2.2 (a-b). Clearly, the presence of fast dynamics in the N-termini and the flexible loops is confirmed and several more isolated low S^2 values indicate local dynamics, in particular in PLAAT4 around residues I92, R111 and N112. The S^2 values for the rigid parts of PLAAT4 are quite high (on average 0.95). It is unclear what the reason is. It is observed for all rigid residues, suggesting that the underlying model of an

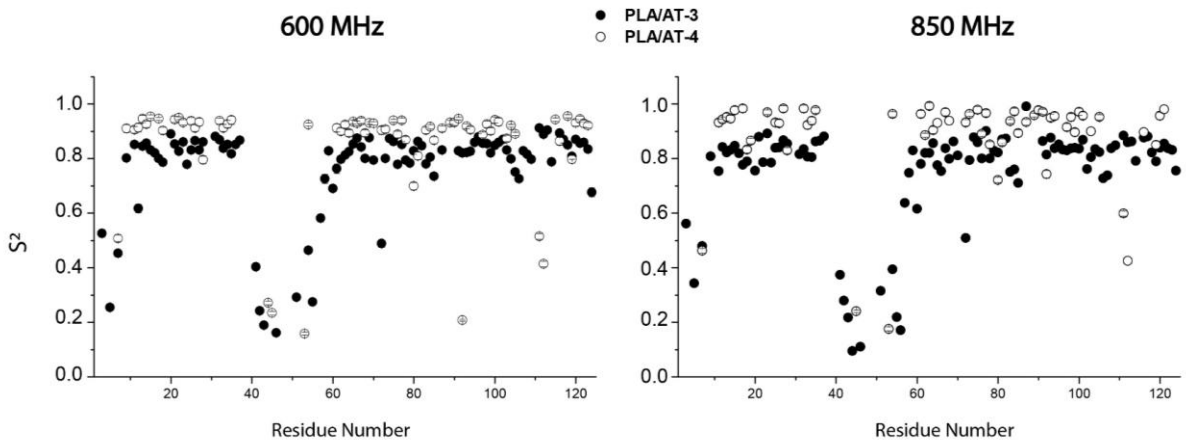

Figure 2.7 Order parameters (S^2) of backbone amides of PLAAT3 (solid circles) and PLAAT4 (open circles) determined from ^{15}N relaxation data obtained at 600 MHz and 850 MHz. An isotropic diffusion tensor was assumed. Errors were estimated using Monte Carlo simulations and represent a 95% confidence level. Most errors in S^2 are smaller than the size of the symbols.

isolated two-spin system in an isotropically rotating protein is not fully valid in the case of PLAAT4. Inclusion of the anisotropy of rotation of the NMR solution structure did not resolve this issue. As will be discussed below, the flexible loop in PLAAT4 assumes on average a more extended conformation than in PLAAT3 and is highly dynamic, which may lead to artificially high τ_c and S^2 values.

Slow motions. To probe backbone motions in the millisecond timescale, we acquired ^{15}N-CPMG relaxation dispersion experiments for both proteins at 14 T and 20 T. Five residues of PLAAT3 showed weak relaxation dispersion (Figure S2.1). Three residues (V50, M51 and D56) are in the highly disordered loop L1, one residue (D81) in the loop joining B5 and A2 and another residue (W24) was in B2 (S3), see Figure 2.6. In contrast, twelve residues of PLAAT4 showed evidence for

millisecond dynamics (Figures 2.8 and S2.2). PLAAT4 has a well-defined dynamic region consisting of 6 residues, R18, L19, Y21, K61 and the catalytic triad members H23 and H35, see Figure 2.6. No resonance could be assigned to C113, the catalytic cysteine. The relaxation data of this region were fitted globally to a two-site exchange model, yielding a population (p_B) of 1% for the minor state and an exchange rate (k_{ex}) of 1.9 (0.2) × 10^3 s^{-1} (Figure 2.8). Dynamic parameters of residues in both PLAAT3 and PLAAT4 are listed in Table S2.3.

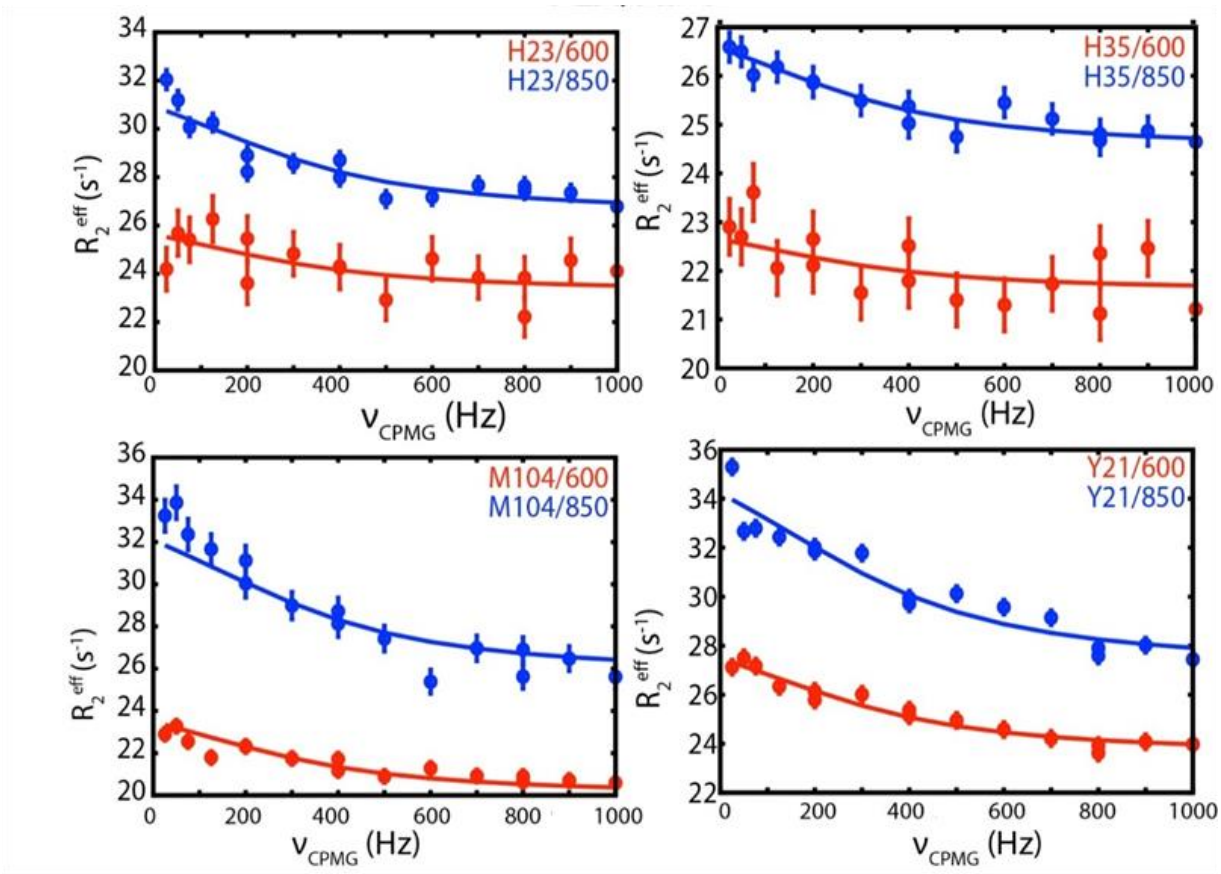

Figure 2.8 Examples of relaxation dispersion curves observed for PLAAT4. The effective transverse relaxation rates are plotted against the CPMG frequency for four residues. The red and blue curves represent data acquired at 14 T and 20 T, respectively. the experimental data are indicated by circles. The errors represent the uncertainties in estimation of effective transverse relaxation rate, based on three duplicate points. The solid lines indicate a fit to the two-state exchange model with a k_{ex} of 1.9 (0.2) × 10^3 s^{-1} and p_B of 1 %. All dispersion curves for PLAAT3 and PLAAT4 are presented in Supplementary Figure S2.3

Discussion

Golczak *et al.* [1] demonstrated that the N-terminal portion of PLAAT4 catalyzes short chain phosphatidylcholines faster than N-terminal portion of PLAAT3 and that the rate of hydrolysis of acyl intermediate is much faster in PLAAT4. Xia *et al.*[12] reported that C-terminal domains (CTDs) of PLAAT4 and PLAAT3 can independently induce HeLa cell death at a comparable level, while their NTDs play opposite roles in regulating the cell death activity of CTDs, even though the structures of PLAAT4N and PLAAT3N are highly similar, with a rmsd of 0.78 Å (PDB entries 2KYT and 2MY9). They hypothesized that such functional difference is probably due to different NTD/CTD interaction patterns between PLAAT4 and PLAAT3. Since the difference should come from the 28% sequence dissimilarity, we studied differences in the dynamics of the NTDs of these proteins. The melting temperature of PLAAT3 is 15 °C higher than that of PLAAT4 and the rotational correlation time is 33% shorter. Thus, PLAAT3 is a more stable and compact protein than PLAAT4. A comparison of the structures shows that the former has a more extensive network of salt bridges dispersed throughout the structure while the latter has lesser salt bridges and that too confined to certain regions, which could explain these observations (Figure 2.5).

Both proteins feature a large loop (L1) that is known to be disordered,[1,11,12,20] and is shown here to be mobile on the pico-nanosecond timescale. It has been proposed that L1 is a membrane anchoring loop in the full length protein.[20] It was shown that replacement of L1 in PLAAT3 by the equivalent loop of LRAT leads to induction of Vitamin A metabolism. This indicates that the highly disordered loop might play a role in modulating activity by interacting with the membrane.

Interesting differences are found between PLAAT3 and PLAAT4 around the active site. PLAAT4 shows low order parameters for R111 and N112, which immediately precede the catalytic nucleophile C113. Since there are no resonance assignments for residues 106-110 and 113-114, we assume that the peaks of these residues are lacking because of broadening due to motional chemical exchange. Millisecond timescale dynamics experiments identified a dynamic active site region involving residues 18, 19, 21, 23, 35 and 61. The resonance of G20 is missing, again indicative of exchange broadening. Residue E22, which forms a salt bridge with R111, shows no broadening due to chemical exchange, which could imply that it either is not dynamic or its change in chemical shift ($\Delta\omega$) happens to be small. Thus, the active site region of PLAAT4 is dynamic, involving at least residues 18-23, 35, 61 and also 113-114. Such a dynamic patch is not observed in PLAAT3. We speculate that the difference in dynamics can explain the activity differences observed PLAAT3 and PLAAT4. The

NTD of PLAAT3 may show little activity toward its substrate due to lack of active site dynamics, whereas the dynamics of PLAAT4 may enable its activity. To develop a model of what the dynamics in PLAAT4 may entail, molecular dynamics simulations can be used. Although they can only sample fast dynamics, they may still provide insight into the nature of motions. Such calculations are known to correlate with NMR relaxation studies.[21–24] These studies are the subject of the next chapter.

Materials and methods

Protein production. DNA sequences encoding the human N-terminal soluble form (residues 1–125) of PLAAT3 or PLAAT4 (Uniprot ID P53816 and Q9UL19, respectively) with N-terminal His_6 tag and a TEV cleavage site were ordered from GeneArt. The fragments were inserted in-frame into bacterial expression vector pET-28a using the *Nco*I and *Xho*I restriction sites. Chemically competent *Escherichia coli* BL21-DE3pLys cells were transformed with the plasmids for protein production. The bacteria were cultured overnight in 50 mL of LB medium with 50 µg/mL kanamycin at 37ºC under shaking. For ^{15}N-labeling, 5 mL of the overnight pre-culture was transferred to 500 mL minimal medium with 50 µg/mL kanamycin. When the OD_{600} reached 0.6, the temperature was lowered to 22ºC and gene expression was induced by addition of 0.5 mM IPTG. The culture was incubated for 5 hours before cells were harvested by centrifugation at 6000 rpm at 4ºC. The pellet was resuspended in 5 mL of 50 mM Tris–HCl buffer (pH 7.5) followed by freezing at -80ºC overnight. The cells were thawed the next day in presence of DNase I and lysozyme and lysed by French press. The lysate was centrifuged at 4ºC at 25000g for 45 min. The supernatant of the cell lysate containing the His_6-tagged soluble protein was then loaded on a HiTrap-Nickel column, equilibrated with 50 mM Tris pH 7.5, 500 mM NaCl and 5 mM Imidazole. The protein was eluted using a linear imidazole concentration gradient from 0 to 0.5 M. The collected fractions were pooled and dialyzed overnight using a 3.5 kDa molecular weight cut-off cellulose membrane at 4ºC in 50 mM Tris, pH 7.5, 500 mM NaCl, 0.5mM EDTA buffer to remove imidazole. His_6-tagged TEV protease was added for the cleavage of the His_6-tag on PLAAT during dialysis overnight. The mixture was loaded again on a His_6-Trap Nickel column to collect the N-terminal PLAAT3 and PLAAT4 domains. The buffer was changed into 50 mM Tris-HCl, 50 mM NaCl, 10 mM DTT, pH 7.5. The volume of the sample was reduced to 2.5 mL using a 5 kDa MWCO Amicon Ultracentrifugal filter (EMD Millipore) at 2200 g and 15°C. The concentrated sample was loaded on and eluted from a Superose12 gel filtration column in 30 mM sodium phosphate buffer with 30 mM NaCl and 10 mM DTT at pH 7.0. All NMR samples contained 1.5 mM uniformly ^{15}N -labeled protein in this buffer with 7% D_2O added for lock.

Thermofluor-based melting temperature (Tm) analysis. Thermofluor analysis was performed on a CFX96 Real-Time PCR system (Bio-Rad) to determine the thermal stability of PLAAT proteins. Duplicate protein samples of 25 µL were prepared in 30 mM sodium phosphate buffer (pH 7.0), 25 mM sodium chloride and 10 mM DTT in 96-well Concord Polycarbonate PCR plates (Bio-Rad) using SYPRO Orange (Sigma-Aldrich) as a fluorescent probe. After sealing with Optical-Quality Sealing Tape (Bio-Rad), plates were vortexed and centrifuged for 30 seconds using an MPS 1000 Mini PCR

Plate Spinner (Labnet). Melting curves were obtained by detection of fluorescence using the FRET channel of the RT-PCR machine. The temperature was increased in steps of 0.5°C increments. At each point, the sample was incubated for 30 s before measuring the fluorescence. At the end the reaction was stopped by heating at 90 °C for 5 min. The results were analyzed in CFX Manager 3.1 (Bio-Rad). The temperature corresponding to the maximum of the first derivative of the melting curve was taken to be the melting temperature (Tm).

T_1, T_2, NOE measurements. NMR experiments were carried out at 25°C on 600 MHz and 850 MHz Bruker Avance III spectrometers equipped with TCI cryoprobes at 600 MHz and 850 MHz proton larmor frequency. Standard Bruker pulse sequences were used for T_1 (hsqct1etf3gpsitc3d), T_2 (hsqct2etf3gpsitc3d) and NOE (hsqcnoef3gpsi) experiments. ^{15}N-^{1}H NOE spectra were acquired first acquired in an interleaved fashion and then split into two HSQCs with and without amide proton saturation each containing 2048/200 points in the ^{1}H/^{15}N dimensions.
In the T_1 and T_2 experiments water saturation was avoided using low power water-flip-back pulses. The mixing times used for the determination of T_1 were 0.01s(x2), 0.16s, 0.22s,0.35s(x2),0.48s,0.6s,0.8s(x2),1.0s,1.2s with duplicates for error estimation. Mixing times for T_2 determination were 0s, 0.034(x2)s, 0.05s, 0.07(x2)s, 0.085s, 0.10, 0.135(x2)s, 0.17s, 0.2(x2)s and 0.24s. All spectra were processed with Bruker TOPSPIN with QSine and Gaussian window functions and linear prediction applied to the ^{15}N dimension. NOE values were calculated as the ratio of peak intensities in the experiment with and without proton saturation. To obtain T_1 and T_2 values the experimental data points (peak heights) were fitted to a curve I_0*exp(-t/T_1 or T_2) where I_0 is the peak intensity of the reference spectra (0s) and fit parameter errors were estimated using Monte Carlo simulations. All NOE, T_1 and T_2 analyses were performed on Bruker Protein Dynamics software suite.

Resonance assignments. ^{1}H-^{15}N HSQC spectra of PLAAT3 and PLAAT4 were assigned using BMRB entries 16883 and 18012, respectively.[15,16]

Relaxation dispersion measurements. Constant relaxation time CPMG experiments were performed for the backbone ^{15}N nuclei of PLAAT3 and PLAAT4 using a modified ST-CW CPMG pulse sequence. A series of two-dimensional (2D) spectra with 1024/60 complex points (^{1}H/^{15}N) were recorded with a relaxation delay (T_{relax}) of 40 ms and cpmg frequencies set to 100, 200(×2), 300, 400(×2), 500, 600, 700, 800(×2), 900 and 1000 Hz, run in an interleaved fashion, followed by a reference spectrum with T_{relax} = 0. Duplicates (x2) were used to estimate the effective transverse

relaxation rate ($R_{2,eff}$) error. The spectra were zero-filled and Fourier transformed with linear prediction applied in the ^{15}N dimension and Gaussian weighting functions applied along the ^{1}H and ^{15}N dimensions, respectively. Peaks were fitted with FuDa (Hansen, http://www.biochem.ucl.ac.uk/hansen/fuda/) to obtain intensities, and $R_{2,eff}$ were calculated from the calculated peak intensities using the formula: $R_{2,eff}(\nu_{CPMG}) = -1/T_{relax} \cdot \ln(I(\nu_{CPMG})/I_0)$, where I_0 is the peak intensity in the reference spectrum. The $R_{2,eff}$ values were corrected for R_1-contribution using the formula described by Jiang *et al.*[25] with 0.95 s^{-1} R_1- and 10.5 s^{-1} as an estimate for R_2-contribution for all residues. Finally, the resulting relaxation dispersion profiles of residues that show dispersion obtained at two fields were fitted to Carver-Richards equation and modeled to a two-state model by using CATIA (Hansen, http://www.biochem.ucl.ac.uk/hansen/catia/), k_{ex} and p_B were obtained as the global output of CATIA whereas $\Delta\omega$ were obtained for individual residues in the fit.

Model-free analysis. Automated model free analysis was performed using Bruker Protein Dynamics software suite. The NH bond length was set to 1.02 Å and the NH chemical shift anisotropy was set to -172 ppm. To ensure good model fitting, calculated errors in T_1, T_2 and NOE were overridden with an error of 2%, as the calculated errors were smaller due to very high signal to noise. The software performs the following actions: Using the two-field T_1, T_2 and NOE datasets, the global correlation time (τ_c) and reduced spectral densities j(0), j(wN), j(0.87wH) were calculated. The reduced spectral densities were then used to estimate the order parameters (S^2), the ratio $D_{\|}/D_{\_}$ of the diffusion tensor and relaxation exchange (R_{ex}) parameters for each residue. Estimation of τ_c required exclusion of dynamic residues which was done by excluding all residues with NOE values less than 0.65 residues with T_2 smaller than the difference between mean and one standard deviation and residues with large T2 values as compared to T1 since these residues might undergo conformational exchange. The T_1, T_2 and NOE values of each residue were fitted to two of 4 models assuming isotropic modelling: M1(S^2) and M2(S^2, τ_e). [18,26–30]

Theoretical calculation of τ_c. Theoretical hydrodynamic calculation to determine the τ_c was done using the program HYDRONMR.[17] Ensemble structures from PDB entries 2KYT and 2MY9 were used as input for atomic coordinates. The effective radius of atomic elements was set to 3.1 Å, the temperature to 25°C and solvent viscosity to 9.1 mP to match our experimental conditions. N-H bonds with explicit hydrogens were chosen as the source of the dipole vectors to calculate the NMR parameters and dipolar couplings. The gyromagnetic ratio of N was set to -2.7126 x 10^7 rad $s^{-1}T^{-1}$, the N-H distance was set to 1.02 Å and the CSA was set to -172 ppm. τ_c was calculated for two

magnetic fields, 14 T and 20 T to match our experimental data. The average τ_c was then calculated from the individual τ_c of each ensemble structures.

Supplementary:

Table S2.1A Relaxation parameters of PLAAT3 obtained from T_1, T_2, and ^{1}H-^{15}N NOE experiments at 600 MHz.

PLAAT3 600 MHz						
Residue	**NOE**	**Error**	**T1[s]**	**Error**	**T2[s]**	**Error**
A3	0.363	0.002	0.658	0.013	0.132	0.003
I5	0.143	0.002	0.705	0.021	0.219	0.007
E7	0.459	0.002	0.639	0.012	0.147	0.003
K9	0.671	0.003	0.704	0.021	0.100	0.006
G11	0.785	0.003	0.740	0.022	0.087	0.003
D12	0.403	0.001	0.685	0.009	0.118	0.002
L13	0.681	0.003	0.747	0.022	0.084	0.003
I14	0.753	0.003	0.732	0.020	0.086	0.002
E15	0.774	0.003	0.717	0.023	0.094	0.004
I16	0.814	0.002	0.742	0.023	0.095	0.003
F17	0.822	0.003	0.706	0.026	0.103	0.005
R18	0.694	0.003	0.772	0.025	0.096	0.003
F20	0.668	0.003	0.716	0.029	0.068	0.003
Y21	0.720	0.002	0.686	0.016	0.092	0.002
R22	0.632	0.002	0.692	0.017	0.094	0.002
H23	0.760	0.003	0.707	0.020	0.089	0.002
W24	0.629	0.002	0.787	0.030	0.093	0.003
A25	0.650	0.003	0.734	0.023	0.088	0.003
I26	0.695	0.002	0.723	0.018	0.083	0.002
Y27	0.808	0.003	0.690	0.025	0.098	0.005
V28	0.705	0.003	0.714	0.020	0.086	0.003
G31	0.757	0.003	0.725	0.022	0.082	0.003
Y32	0.723	0.002	0.700	0.015	0.087	0.002
V33	0.728	0.003	0.733	0.022	0.090	0.003
V34	0.713	0.003	0.738	0.022	0.085	0.002
H35	0.689	0.002	0.705	0.021	0.096	0.003
L36	0.737	0.003	0.716	0.020	0.089	0.003
A37	0.681	0.002	0.699	0.018	0.086	0.002
E41	0.194	0.003	0.686	0.046	0.162	0.009
V42	-0.103	0.001	0.715	0.012	0.230	0.004
A43	-0.379	0.002	0.774	0.020	0.274	0.009
G44	-1.095	0.006	1.136	0.119	0.000	0.000
G46	-0.683	0.004	0.945	0.061	0.317	0.024
M51	-0.090	0.002	0.716	0.017	0.206	0.004
L54	0.323	0.002	0.680	0.015	0.147	0.002
T55	0.101	0.002	0.673	0.035	0.207	0.008
D56	-1.190	0.009	0.993	0.129	0.000	0.000
K57	0.534	0.001	0.700	0.012	0.128	0.002
A58	0.539	0.002	0.672	0.012	0.103	0.002
I59	0.645	0.003	0.702	0.017	0.093	0.002
V60	0.354	0.002	0.759	0.017	0.113	0.003
K61	0.693	0.003	0.669	0.021	0.101	0.004
K62	0.712	0.002	0.752	0.016	0.096	0.002
E63	0.648	0.002	0.731	0.016	0.093	0.003
L64	0.676	0.002	0.759	0.017	0.087	0.002
L65	0.767	0.003	0.705	0.022	0.091	0.003
Y66	0.717	0.002	0.681	0.017	0.088	0.002
D67	0.676	0.002	0.707	0.014	0.090	0.002

V68	0.724	0.002	0.748	0.016	0.096	0.002
A69	0.714	0.002	0.685	0.014	0.087	0.002
G70	0.692	0.002	0.706	0.017	0.101	0.002
D72	0.287	0.001	0.758	0.010	0.147	0.002
K73	0.739	0.002	0.740	0.016	0.098	0.002
Y74	0.769	0.003	0.714	0.023	0.085	0.003
Q75	0.745	0.003	0.714	0.024	0.087	0.003
V76	0.680	0.002	0.766	0.016	0.098	0.002
N77	0.753	0.003	0.702	0.016	0.091	0.002
N78	0.731	0.002	0.779	0.015	0.094	0.002
K79	0.644	0.002	0.744	0.019	0.098	0.002
H80	0.703	0.002	0.685	0.017	0.097	0.002
D81	0.709	0.002	0.703	0.015	0.088	0.002
D82	0.710	0.002	0.695	0.014	0.092	0.002
K83	0.698	0.002	0.778	0.016	0.096	0.002
Y84	0.696	0.002	0.740	0.013	0.095	0.002
S85	0.668	0.002	0.785	0.014	0.107	0.002
L87	0.677	0.002	0.718	0.017	0.091	0.003
K91	0.670	0.002	0.740	0.018	0.089	0.002
I92	0.695	0.003	0.765	0.021	0.088	0.002
I93	0.686	0.003	0.758	0.019	0.088	0.002
Q94	0.732	0.002	0.726	0.013	0.093	0.002
R95	0.714	0.002	0.712	0.013	0.087	0.002
A96	0.767	0.002	0.728	0.013	0.082	0.002
E97	0.744	0.003	0.737	0.016	0.085	0.002
E98	0.709	0.002	0.734	0.012	0.085	0.001
L99	0.679	0.002	0.767	0.018	0.087	0.002
V100	0.720	0.002	0.738	0.014	0.086	0.002
G101	0.721	0.003	0.688	0.025	0.091	0.003
Q102	0.677	0.002	0.723	0.013	0.080	0.002
E103	0.726	0.001	0.719	0.007	0.093	0.001
V104	0.653	0.003	0.727	0.019	0.097	0.003
L105	0.665	0.002	0.720	0.018	0.109	0.003
Y106	0.529	0.002	0.733	0.015	0.111	0.002
K107	0.655	0.002	0.695	0.017	0.094	0.002
L108	0.679	0.002	0.720	0.016	0.095	0.003
T109	0.646	0.003	0.757	0.022	0.093	0.003
E111	0.761	0.003	0.669	0.024	0.083	0.003
N112	0.708	0.002	0.675	0.016	0.085	0.002
C113	0.721	0.002	0.656	0.017	0.084	0.002
E114	0.486	0.002	0.702	0.018	0.096	0.002
F116	0.747	0.003	0.702	0.018	0.082	0.002
V117	0.729	0.003	0.679	0.021	0.090	0.003
N118	0.689	0.002	0.685	0.014	0.092	0.002
E119	0.596	0.002	0.723	0.015	0.093	0.002
L120	0.769	0.002	0.703	0.015	0.088	0.002
R121	0.777	0.003	0.716	0.018	0.089	0.002
Y122	0.753	0.003	0.711	0.020	0.088	0.002
G123	0.737	0.003	0.710	0.017	0.094	0.002
V124	0.589	0.002	0.693	0.016	0.113	0.002

Table S2.1B Relaxation parameters of PLAAT3 obtained from T_1, T_2, and ^{1}H-^{15}N NOE experiments at 850 MHz.

PLAAT3 850 MHz						
Residue	**NOE**	**Error**	**T1[s]**	**Error**	**T2[s]**	**Error**
A3	0.630	0.001	0.851	0.012	0.112	0.002
I5	0.161	0.001	0.845	0.032	0.160	0.001
E7	0.592	0.001	0.858	0.013	0.129	0.002
K9	0.876	0.002	1.055	0.007	0.084	0.002
G11	0.469	0.001	1.164	0.050	0.073	0.000
D12	0.818	0.001	0.951	0.017	0.083	0.001
L13	0.888	0.002	1.137	0.034	0.077	0.001
I14	0.867	0.002	1.134	0.037	0.075	0.000
E15	0.892	0.002	1.107	0.010	0.074	0.001
I16	0.885	0.002	1.137	0.017	0.077	0.001
F17	0.885	0.002	1.115	0.016	0.087	0.001
R18	0.842	0.001	1.189	0.028	0.078	0.001
F20	0.406	0.001	1.073	0.016	0.049	0.000
Y21	0.835	0.001	1.008	0.034	0.074	0.001
R22	0.765	0.002	1.033	0.007	0.087	0.001
H23	0.854	0.002	1.057	0.037	0.069	0.001
W24	0.841	0.002	1.258	0.016	0.073	0.001
A25	0.860	0.002	1.167	0.023	0.070	0.001
I26	0.853	0.001	1.114	0.078	0.074	0.001
Y27	0.881	0.002	1.025	0.043	0.076	0.001
V28	0.849	0.002	1.039	0.033	0.077	0.002
G31	0.863	0.002	1.148	0.040	0.077	0.002
Y32	0.877	0.002	1.077	0.009	0.078	0.001
V33	0.864	0.002	1.155	0.043	0.078	0.001
V34	0.852	0.002	1.158	0.009	0.078	0.001
H35	0.872	0.002	1.110	0.020	0.071	0.001
L36	0.883	0.002	1.073	0.017	0.073	0.001
A37	0.830	0.002	1.072	0.015	0.069	0.001
E41	0.184	0.001	0.867	0.050	0.151	0.004
V42	0.148	0.001	0.809	0.004	0.184	0.003
A43	0.061	0.001	0.824	0.014	0.222	0.004
G44	-0.425	0.002	1.071	0.033	0.395	0.009
G46	-0.106	0.002	0.992	0.034	0.347	0.021
M51	0.250	0.001	0.838	0.024	0.171	0.002
L54	0.498	0.001	0.850	0.011	0.148	0.005
T55	0.368	0.001	0.795	0.043	0.215	0.001
D56	-0.353	0.002	1.015	0.022	0.279	0.005
K57	0.685	0.001	0.927	0.006	0.105	0.000
A58	0.705	0.001	0.942	0.005	0.090	0.001
I59	0.827	0.002	1.064	0.024	0.079	0.001
V60	0.669	0.001	1.043	0.021	0.121	0.002
K61	0.480	0.001	1.013	0.017	0.080	0.002
K62	0.834	0.001	1.164	0.028	0.074	0.001
E63	0.847	0.001	1.128	0.018	0.077	0.001
L64	0.859	0.001	1.115	0.014	0.071	0.001
L65	0.464	0.001	1.063	0.030	0.072	0.001
Y66	0.414	0.001	1.025	0.019	0.078	0.001
D67	0.895	0.001	1.080	0.024	0.078	0.000
V68	0.842	0.001	1.116	0.015	0.082	0.002
A69	0.882	0.002	1.013	0.007	0.077	0.001
G70	0.868	0.001	1.103	0.017	0.081	0.001
D72	0.483	0.001	0.989	0.021	0.129	0.002

K73	0.850	0.002	1.097	0.010	0.084	0.000
Y74	0.889	0.002	1.060	0.029	0.072	0.000
Q75	0.865	0.002	1.110	0.051	0.071	0.001
V76	0.798	0.002	1.125	0.030	0.080	0.001
N77	0.880	0.002	1.062	0.019	0.068	0.001
N78	0.879	0.002	1.212	0.042	0.075	0.001
K79	0.834	0.001	1.124	0.009	0.075	0.001
H80	0.815	0.001	1.022	0.013	0.083	0.001
D81	0.880	0.002	1.082	0.007	0.072	0.000
D82	0.840	0.001	1.027	0.008	0.074	0.001
K83	0.809	0.001	1.177	0.022	0.087	0.000
Y84	0.826	0.001	1.133	0.032	0.088	0.001
S85	0.759	0.001	1.185	0.020	0.094	0.001
L87	0.790	0.002	1.062	0.010	0.077	0.001
K91	0.865	0.001	1.134	0.026	0.068	0.001
I92	0.868	0.002	1.151	0.015	0.077	0.001
I93	0.857	0.002	1.107	0.023	0.068	0.001
Q94	0.831	0.001	1.076	0.005	0.077	0.000
R95	0.826	0.001	1.067	0.006	0.075	0.000
A96	0.867	0.001	1.116	0.005	0.076	0.000
E97	0.856	0.001	1.162	0.010	0.072	0.000
E98	0.862	0.001	1.112	0.010	0.075	0.001
L99	0.846	0.001	1.134	0.035	0.073	0.001
V100	0.849	0.001	1.119	0.008	0.074	0.001
G101	0.861	0.002	1.041	0.014	0.074	0.002
Q102	0.432	0.001	1.061	0.024	0.073	0.001
E103	0.835	0.001	1.085	0.011	0.082	0.000
V104	0.786	0.002	1.075	0.010	0.077	0.001
L105	0.741	0.001	0.988	0.018	0.083	0.000
Y106	0.359	0.001	1.015	0.018	0.085	0.002
K107	0.378	0.001	1.006	0.026	0.074	0.001
L108	0.783	0.002	1.092	0.028	0.075	0.001
T109	0.748	0.002	1.073	0.021	0.073	0.001
E111	0.858	0.002	1.002	0.008	0.074	0.001
N112	0.841	0.002	1.039	0.031	0.076	0.001
C113	0.866	0.002	0.999	0.036	0.078	0.001
E114	0.793	0.001	1.040	0.013	0.087	0.001
F116	0.865	0.002	1.028	0.014	0.074	0.001
V117	0.891	0.002	1.020	0.020	0.074	0.001
N118	0.751	0.001	1.017	0.035	0.082	0.000
E119	0.822	0.001	1.050	0.005	0.087	0.001
L120	0.863	0.002	1.080	0.008	0.077	0.001
R121	0.879	0.002	1.086	0.041	0.074	0.001
Y122	0.875	0.002	1.111	0.027	0.075	0.000
G123	0.859	0.002	1.107	0.037	0.077	0.001
V124	0.767	0.001	0.984	0.019	0.095	0.001

Table S2.1C Relaxation parameters of PLAAT4 obtained from T_1, T_2, and ^{1}H-^{15}N NOE experiments at 600 MHz.

PLAAT4 **600 MHz**						
Residue	**NOE**	**Error**	**T1[s]**	**Error**	**T2[s]**	**Error**

E7	0.338	0.003	0.752	0.041	0.099	0.002
K9	0.724	0.004	0.893	0.048	0.060	0.002
G11	0.756	0.005	0.923	0.039	0.061	0.002
D12	0.727	0.003	0.845	0.030	0.057	0.002
L13	0.800	0.004	0.937	0.056	0.055	0.002
I14	0.748	0.005	0.918	0.028	0.058	0.001
E15	0.779	0.005	0.886	0.062	0.054	0.002
F17	0.765	0.005	0.892	0.036	0.057	0.002
R18	0.720	0.006	0.922	0.046	0.060	0.002
L19	0.693	0.004	0.878	0.080	0.000	0.000
Y21	0.755	0.005	0.866	0.045	0.054	0.003
E22	0.745	0.006	0.892	0.047	0.047	0.000
H23	0.731	0.006	0.877	0.049	0.056	0.003
A25	0.785	0.005	0.920	0.038	0.057	0.002
L26	0.750	0.005	0.952	0.058	0.058	0.002
Y27	0.795	0.005	0.879	0.050	0.059	0.003
I28	0.525	0.003	0.876	0.040	0.068	0.004
Y32	0.741	0.003	0.933	0.047	0.054	0.003
V33	0.763	0.005	0.932	0.060	0.059	0.003
I34	0.775	0.004	0.925	0.034	0.058	0.002
H35	0.759	0.006	0.863	0.044	0.056	0.003
G44	0.094	0.005	0.750	0.027	0.162	0.015
A45	0.076	0.003	0.775	0.044	0.181	0.008
V53	-0.718	0.002	0.879	0.027	0.247	0.014
L54	0.701	0.003	0.909	0.018	0.054	0.003
K61	0.741	0.006	0.839	0.035	0.057	0.002
R62	0.734	0.005	0.925	0.047	0.061	0.004
E63	0.755	0.005	0.921	0.054	0.058	0.002
R64	0.713	0.003	0.966	0.029	0.059	0.003
L65	0.734	0.004	0.909	0.023	0.056	0.002
E66	0.727	0.004	0.888	0.029	0.058	0.002
D67	0.751	0.004	0.924	0.043	0.055	0.002
V68	0.743	0.004	0.992	0.032	0.057	0.002
V69	0.711	0.004	0.900	0.028	0.052	0.003
G70	0.716	0.004	0.891	0.035	0.056	0.002
C72	0.713	0.004	0.877	0.028	0.060	0.002
C73	0.719	0.006	0.953	0.053	0.058	0.004
R75	0.746	0.006	0.894	0.124	0.056	0.003
V76	0.702	0.004	0.930	0.036	0.062	0.002
N77	0.750	0.004	0.883	0.042	0.056	0.003
N78	0.744	0.003	0.962	0.027	0.063	0.002
L80	0.411	0.002	0.821	0.043	0.075	0.001
D81	0.598	0.003	0.829	0.044	0.065	0.002
E83	0.690	0.004	0.916	0.035	0.060	0.002
Y84	0.693	0.004	0.913	0.025	0.057	0.001
Q85	0.684	0.003	0.939	0.047	0.064	0.002
R87	0.686	0.003	0.927	0.033	0.058	0.003
V89	0.729	0.003	0.910	0.058	0.056	0.002
E90	0.733	0.003	0.940	0.013	0.054	0.001
V91	0.766	0.004	0.895	0.047	0.056	0.001
I92	0.217	0.003	1.179	0.050	0.306	0.020
I93	0.695	0.004	0.937	0.044	0.054	0.004
S94	0.705	0.003	0.948	0.023	0.058	0.002
K97	0.637	0.004	0.958	0.052	0.058	0.001
E98	0.773	0.004	0.957	0.024	0.056	0.002

M99	0.728	0.004	0.943	0.047	0.059	0.002
V100	0.754	0.004	0.953	0.081	0.052	0.002
G101	0.778	0.006	0.875	0.069	0.058	0.004
K103	0.659	0.003	0.926	0.039	0.063	0.004
M104	0.689	0.004	0.911	0.043	0.053	0.004
K105	0.621	0.004	0.921	0.028	0.058	0.001
R111	0.235	0.004	0.811	0.062	0.100	0.011
N112	0.231	0.003	0.729	0.034	0.116	0.006
H115	0.748	0.006	0.885	0.042	0.054	0.003
F116	0.701	0.003	0.866	0.028	0.064	0.001
T118	0.769	0.006	0.907	0.099	0.049	0.000
Q119	0.567	0.002	0.861	0.024	0.068	0.001
L120	0.740	0.004	0.952	0.038	0.054	0.003
R121	0.759	0.005	0.932	0.079	0.053	0.002
Y122	0.800	0.006	0.967	0.046	0.055	0.002
G123	0.716	0.005	0.905	0.032	0.059	0.004

Table S2.1D Relaxation parameters of PLAAT4 obtained from T_1, T_2, and ^{1}H-^{15}N NOE experiments at 850 MHz.

PLAAT4 **850 MHz**						
Residue	**NOE**	**Error**	**T1[s]**	**Error**	**T2[s]**	**Error**
E7	0.542	0.003	0.917	0.039	0.092	0.003
K9	0.838	0.003	1.361	0.040	0.000	0.000
G11	0.877	0.004	1.428	0.051	0.047	0.000
D12	0.849	0.002	1.260	0.013	0.045	0.000
L13	0.874	0.003	1.449	0.075	0.044	0.000
I14	0.894	0.004	1.431	0.020	0.046	0.000
E15	0.888	0.004	1.397	0.073	0.044	0.000
F17	0.916	0.004	1.418	0.058	0.043	0.000
R18	0.777	0.005	1.510	0.053	0.054	0.002
L19	0.838	0.003	1.273	0.056	0.057	0.005
Y21	0.867	0.004	1.264	0.058	0.000	0.000
E22	0.845	0.004	1.330	0.086	0.000	0.000
H23	0.843	0.005	1.377	0.048	0.044	0.000
A25	0.899	0.004	1.453	0.073	0.047	0.000
L26	0.870	0.004	1.497	0.054	0.045	0.000
Y27	0.882	0.004	1.335	0.057	0.043	0.000
I28	0.681	0.002	1.292	0.113	0.057	0.002
Y32	0.883	0.003	1.420	0.021	0.042	0.000
V33	0.857	0.004	1.456	0.062	0.047	0.000
I34	0.846	0.003	1.438	0.100	0.046	0.000
H35	0.889	0.004	1.343	0.025	0.045	0.000
A45	0.411	0.003	0.858	0.048	0.152	0.010
V53	-0.125	0.001	0.931	0.014	0.195	0.005
L54	0.819	0.003	1.377	0.047	0.044	0.000
K61	0.867	0.004	1.319	0.040	0.045	0.000
R62	0.833	0.003	1.486	0.062	0.049	0.001
E63	0.879	0.003	1.406	0.035	0.005	0.000
R64	0.834	0.003	1.501	0.043	0.047	0.000
L65	0.864	0.004	1.426	0.035	0.047	0.000

E66	0.850	0.003	1.311	0.046	0.000	0.000
D67	0.864	0.003	1.424	0.068	0.043	0.000
V68	0.858	0.003	1.478	0.024	0.045	0.000
V69	0.881	0.003	1.373	0.026	0.000	0.000
G70	0.838	0.003	1.344	0.026	0.000	0.000
C72	0.788	0.003	1.321	0.057	0.047	0.000
C73	0.834	0.004	1.391	0.070	0.044	0.000
R75	0.866	0.004	1.367	0.129	0.044	0.000
V76	0.833	0.003	1.399	0.072	0.051	0.001
N77	0.877	0.003	1.325	0.065	0.045	0.000
N78	0.854	0.003	1.485	0.059	0.053	0.002
L80	0.607	0.002	1.070	0.027	0.059	0.002
D81	0.765	0.003	1.203	0.057	0.052	0.002
E83	0.788	0.003	1.363	0.091	0.047	0.000
Y84	0.850	0.003	1.367	0.040	0.044	0.000
Q85	0.759	0.003	1.387	0.038	0.051	0.001
R87	0.810	0.002	1.433	0.023	0.046	0.000
V89	0.842	0.003	1.346	0.026	0.046	0.000
E90	0.859	0.003	1.351	0.011	0.043	0.000
V91	0.863	0.003	1.391	0.030	0.044	0.000
I92	0.641	0.003	1.346	0.131	0.067	0.004
I93	0.860	0.003	1.445	0.056	0.045	0.000
S94	0.842	0.003	1.391	0.019	0.045	0.000
K97	0.821	0.003	1.501	0.036	0.046	0.000
E98	0.860	0.002	1.437	0.027	0.045	0.000
M99	0.837	0.003	1.465	0.029	0.049	0.000
V100	0.864	0.003	1.472	0.054	0.041	0.000
G101	0.870	0.005	1.362	0.044	0.046	0.000
K103	0.767	0.003	1.415	0.025	0.049	0.000
M104	0.755	0.005	1.389	0.100	0.000	0.000
K105	0.795	0.004	1.366	0.052	0.046	0.000
R111	0.514	0.004	1.106	0.116	0.077	0.008
N112	0.456	0.003	0.889	0.024	0.096	0.004
H115	0.853	0.006	1.390	0.363	0.000	0.000
F116	0.801	0.002	1.285	0.049	0.051	0.001
T118	0.917	0.006	1.401	0.104	0.000	0.000
Q119	0.747	0.002	1.272	0.035	0.056	0.001
L120	0.867	0.003	1.471	0.069	0.043	0.000
R121	0.875	0.004	1.429	0.084	0.042	0.000
Y122	0.883	0.004	1.461	0.130	0.000	0.000
G123	0.844	0.004	1.372	0.064	0.000	0.000

Table S2.2A S^2 and τ_e values of PLAAT3 obtained from the model free fit of the relaxation parameters of individual residues obtained at 600 MHz and 850 MHz. M2 and TM2 corresponds to isotropic and anisotropic model free calculations using model 2.

PLAAT3									
600 MHz					850 MHz				
Res	S^2 (M2)	S^2 (TM2)	T_e (M2)	Error	Res	S^2 (M2)	S^2 (TM2)	T_e (M2)	Error
3	0.526	0.527	6.53E-10	2.02e-11	3	0.562	0.575	6E-10	1.75E-11
5	0.254	0.255	7.2E-10	6.99e-12	5	0.343	0.336	4.07E-10	4.56E-12
7	0.453	0.438	8.56E-10	2.00e-11	7	0.479	0.454	6.03E-10	1.38E-11
9	0.802	0.803	7.05E-11	7.43e-12	9	0.808	0.799	1.13E-11	3.28E-12
11	0.851	0.85	4.38E-11	7.50e-12	11	0.754	0.76	8.73E-11	8.61E-12
12	0.618	0.598	5.62E-10	2.75e-11	12	0.843	0.805	3.06E-11	5.02E-12
13	0.845	0.847	9.01E-11	1.26e-11	13	0.822	0.821	6.67E-12	3.51E-12
14	0.856	0.855	6.07E-11	9.34e-12	14	0.831	0.829	1.12E-11	3.74E-12
15	0.832	0.83	4.39E-11	6.54e-12	15	0.847	0.846	7E-12	4.24E-12
16	0.82	0.817	2.69E-11	5.25e-12	16	0.819	0.817	7.41E-12	3.44E-12
17	0.801	0.801	2.37E-11	4.62e-12	17	0.778	0.776	7.55E-12	2.69E-12
18	0.786	0.785	5.34E-11	5.37e-12	18	0.79	0.79	1.28E-11	2.85E-12
20	0.89	0.889	1.88E-10	7.39e-11	20	0.756	0.753	1.38E-10	2.3E-11
21	0.854	0.812	8.16E-11	1.22e-11	21	0.879	0.88	3.1E-11	6.69E-12
22	0.827	0.827	1.1E-10	1.52e-11	22	0.787	0.787	2.94E-11	3.36E-12
23	0.861	0.86	6.17E-11	9.92e-12	23	0.892	0.89	2.4E-11	6.87E-12
24	0.779	0.78	7.05E-11	6.42e-12	24	0.785	0.789	1.09E-11	2.71E-12
25	0.832	0.834	9.94E-11	1.33e-11	25	0.839	0.836	1.18E-11	3.95E-12
26	0.865	0.867	1.03E-10	1.77e-11	26	0.841	0.841	1.56E-11	4.11E-12
27	0.832	0.827	3.37E-11	6.03e-12	27	0.868	0.862	1.41E-11	5.18E-12
28	0.861	0.861	9.32E-11	1.50e-11	28	0.855	0.852	2.1E-11	4.84E-12
31	0.882	0.885	7.52E-11	1.40e-11	31	0.816	0.815	1.11E-11	3.38E-12
32	0.869	0.868	9.03E-11	1.53e-11	32	0.835	0.833	1.13E-11	3.91E-12
33	0.838	0.838	6.35E-11	8.49e-12	33	0.807	0.805	1.04E-11	3.17E-12
34	0.851	0.851	7.76E-11	1.12e-11	34	0.805	0.805	1.25E-11	3.14E-12
35	0.818	0.817	7.17E-11	8.32e-12	35	0.862	0.862	1.21E-11	4.78E-12
36	0.852	0.849	6.78E-11	9.92e-12	36	0.865	0.864	1.12E-11	4.95E-12
37	0.868	0.869	1.26E-10	2.52e-11	37	0.882	0.882	2.96E-11	6.62E-12
41	0.403	0.4	6.32E-10	1.19e-11	41	0.374	0.373	4.02E-10	5.18E-12
42	0.242	0.242	5.79E-10	6.09e-12	42	0.28	0.273	4.29E-10	3.6E-12
43	0.189	0.18	4.94E-10	5.50e-12	43	0.217	0.21	4.18E-10	2.52E-12
					44	0.0942	0.0917	3.2E-10	2.16E-12
46	0.162	0.167	4.06E-10	5.65e-12	46	0.11	0.111	3.97E-10	1.48E-12
51	0.291	0.3	5.48E-10	7.34e-12	51	0.315	0.299	4.63E-10	4.68E-12
54	0.464	0.443	6.83E-10	1.60e-11	54	0.394	0.374	5.75E-10	9.83E-12
55	0.275	0.279	6.75E-10	7.33e-12	55	0.219	0.227	5.67E-10	5.65E-12
					56	0.17	0.176	3.12E-10	2.5E-12
57	0.582	0.58	7.75E-10	2.79e-11	57	0.638	0.655	5.65E-10	2.05E-11
58	0.726	0.695	5.42E-10	4.56e-11	58	0.748	0.773	4.91E-10	2.86E-11
59	0.829	0.827	1.02E-10	1.36e-11	59	0.83	0.828	2.23E-11	4.03E-12
60	0.69	0.689	1.12E-10	8.21e-12	60	0.616	0.616	2.11E-11	1.33E-12
61	0.763	0.723	7.53E-10	6.23e-11	61	0.781	0.783	1.37E-10	2.61E-11
62	0.797	0.795	5.22E-11	5.65e-12	62	0.82	0.822	1.65E-11	3.52E-12
63	0.813	0.812	8.54E-11	9.69e-12	63	0.821	0.819	1.52E-11	3.55E-12
64	0.826	0.825	7.81E-11	9.38e-12	64	0.857	0.857	1.52E-11	4.64E-12

65	0.853	0.852	5.48E-11	8.59e-12	65	0.776	0.776	1.26E-10	2.05E-11
66	0.875	0.874	1.05E-10	1.99e-11	66	0.754	0.758	1.43E-10	2.54E-11
67	0.843	0.842	9.61E-11	1.37e-11	67	0.838	0.836	7.48E-12	3.99E-12
68	0.801	0.8	5E-11	5.65e-12	68	0.799	0.796	1.51E-11	3.09E-12
69	0.877	0.876	1.1E-10	2.17e-11	69	0.863	0.866	1.4E-11	4.97E-12
70	0.795	0.794	6.02E-11	6.23e-12	70	0.811	0.812	1.14E-11	3.31E-12
72	0.488	0.488	6.17E-10	1.59e-11	72	0.509	0.526	4.83E-10	1.03E-11
73	0.801	0.8	4.56E-11	5.39e-12	73	0.795	0.791	1.39E-11	3.01E-12
74	0.874	0.874	6.38E-11	1.14e-11	74	0.878	0.876	1.06E-11	5.53E-12
75	0.863	0.863	7.05E-11	1.13e-11	75	0.859	0.856	1.4E-11	4.7E-12
76	0.779	0.777	5.57E-11	5.32e-12	76	0.8	0.8	2.29E-11	3.29E-12
77	0.851	0.852	6.09E-11	9.14e-12	77	0.902	0.9	1.46E-11	7.11E-12
78	0.795	0.793	4.46E-11	5.09e-12	78	0.8	0.802	6.04E-12	3.01E-12
79	0.784	0.781	6.98E-11	6.59e-12	79	0.828	0.828	1.85E-11	3.78E-12
80	0.828	0.829	7.23E-11	8.96e-12	80	0.823	0.819	2.55E-11	4E-12
81	0.862	0.861	9.33E-11	1.52e-11	81	0.871	0.872	1.18E-11	5.21E-12
82	0.847	0.848	8.08E-11	1.14e-11	82	0.874	0.873	2.73E-11	6.04E-12
83	0.781	0.781	5.05E-11	5.03e-12	83	0.751	0.751	1.61E-11	2.33E-12
84	0.805	0.804	6.09E-11	6.59e-12	84	0.761	0.761	1.51E-11	2.47E-12
85	0.736	0.735	4.64E-11	3.78e-12	85	0.71	0.704	1.94E-11	1.94E-12
87	0.831	0.83	8.49E-11	1.08e-11	87	0.992	0.971	4.31E-10	9.55E-10
91	0.828	0.828	8.37E-11	1.03e-11	91	0.864	0.867	1.29E-11	4.81E-12
92	0.821	0.823	6.72E-11	7.90e-12	92	0.815	0.815	9.99E-12	3.34E-12
93	0.822	0.823	7.16E-11	8.42e-12	93	0.876	0.875	1.77E-11	5.53E-12
94	0.827	0.827	5.76E-11	7.35e-12	94	0.838	0.837	2.2E-11	4.23E-12
95	0.86	0.86	8.7E-11	1.36e-11	95	0.851	0.85	2.53E-11	4.85E-12
96	0.879	0.878	6.56E-11	1.20e-11	96	0.833	0.832	1.19E-11	3.83E-12
97	0.857	0.857	6.5E-11	9.95e-12	97	0.83	0.832	1.25E-11	3.7E-12
98	0.855	0.852	8.3E-11	1.23e-11	98	0.838	0.838	1.34E-11	3.99E-12
99	0.821	0.822	7.38E-11	8.59e-12	99	0.84	0.837	1.65E-11	4.06E-12
100	0.848	0.847	7.21E-11	1.01e-11	100	0.837	0.834	1.61E-11	3.98E-12
101	0.859	0.856	8.42E-11	1.31e-11	101	0.869	0.864	1.93E-11	5.34E-12
102	0.871	0.873	1.28E-10	2.64e-11	102	0.762	0.764	1.3E-10	2.09E-11
103	0.831	0.828	6.21E-11	7.99e-12	103	0.805	0.806	1.76E-11	3.27E-12
104	0.799	0.799	7.47E-11	7.68e-12	104	0.834	0.832	3.23E-11	4.65E-12
105	0.751	0.753	5.26E-11	4.46e-12	105	0.824	0.82	4.47E-11	5.47E-12
106	0.726	0.728	7.84E-11	5.66e-12	106	0.727	0.727	1.54E-10	2.64E-11
107	0.829	0.789	9.67E-11	1.26e-11	107	0.739	0.743	1.53E-10	2.77E-11
108	0.816	0.812	7.37E-11	8.38e-12	108	0.838	0.838	3.34E-11	4.87E-12
109	0.798	0.798	7.51E-11	7.62e-12	109	0.848	0.848	4.7E-11	6.57E-12
111	0.913	0.913	1.25E-10	3.88e-11	111	0.885	0.881	2.48E-11	6.6E-12
112	0.889	0.872	1.45E-10	4.04e-11	112	0.859	0.859	2.36E-11	5.12E-12
113	0.904	0.904	2.14E-10	1.26e-10	113	0.862	0.864	1.9E-11	5.08E-12
114	0.788	0.753	1.82E-10	3.63e-11	114	0.791	0.794	2.49E-11	3.25E-12
116	0.894	0.895	9.79E-11	2.13e-11	116	0.876	0.872	1.97E-11	5.74E-12
117	0.87	0.84	9.07E-11	1.57e-11	117	0.882	0.877	1.23E-11	5.81E-12
118	0.85	0.805	9.7E-11	1.46e-11	118	0.822	0.824	4.03E-11	4.95E-12
119	0.809	0.807	1.09E-10	1.33e-11	119	0.79	0.782	1.94E-11	3.05E-12
120	0.87	0.868	6.3E-11	1.09e-11	120	0.84	0.839	1.46E-11	4.08E-12
121	0.856	0.856	5.08E-11	8.40e-12	121	0.855	0.854	1.11E-11	4.54E-12
122	0.86	0.86	6.49E-11	1.02e-11	122	0.838	0.837	1.05E-11	3.96E-12
123	0.834	0.83	5.94E-11	7.91e-12	123	0.831	0.829	1.4E-11	3.8E-12
124	0.677	0.648	7.11E-10	3.91e-11	124	0.755	0.71	2.55E-11	2.7E-12

Table S2.2B S^2 and τ_e values of PLAAT4 obtained from the model free fit of the relaxation parameters of individual residues obtained at 600 MHz and 850 MHz. M2 and TM2 corresponds to isotropic and anisotropic model free calculations using model 2.

PLAAT4									
600 MHz					850 MHz				
Res	S^2 (M2)	S^2 (TM2)	T_e (M2)	Error	Res	S^2 (M2)	S^2 (TM2)	T_e (M2)	Error
7	0.508	0.524	7.23E-10	1.28e-11	7	0.463	0.476	6.18E-10	1.06e-11
9	0.91	0.916	4.24E-10	1.15e-10					-
11	0.906	0.905	7.65E-11	1.60e-11	11	0.932	0.932	2.16E-11	8.26e-12
12	0.914	0.881	4.54E-10	1.25e-10	12	0.943	0.942	6.02E-10	1.10e-10
13	0.946	0.946	9.6E-11	3.74e-11	13	0.953	0.951	2.99E-11	1.38e-11
14	0.926	0.925	1.17E-10	3.71e-11	14	0.946	0.945	1.69E-11	9.76e-12
15	0.954	0.953	2.4E-10	2.38e-10	15	0.978	0.977	5.11E-11	4.52e-11
17	0.946	0.945	2.2E-10	1.77e-10	17	0.984	0.984	9.68E-12	3.34e-11
18	0.903	0.902	9.8E-11	2.12e-11	18	0.833	0.834	2.42E-11	3.15e-12
				-	19	0.865	0.876	6.02E-10	4.53e-11
21	0.944	0.933	2.8E-10	2.21e-10					-
22	0.949	0.949	2.31E-10	2.04e-10					-
23	0.933	0.922	2.72E-10	1.79e-10	23	0.97	0.97	1.26E-10	1.30e-10
25	0.938	0.937	1E-10	3.47e-11	25	0.932	0.931	1.12E-11	7.31e-12
26	0.912	0.911	8.48E-11	1.93e-11	26	0.93	0.929	2.02E-11	7.72e-12
27	0.934	0.948	5.48E-10	1.58e-10	27	0.983	0.982	2.88E-10	3.15e-10
28	0.796	0.807	4.84E-10	4.31e-11	28	0.83	0.843	4.26E-10	2.64e-11
32	0.938	0.939	1.66E-10	8.46e-11	32	0.983	0.984	6.98E-11	8.50e-11
33	0.913	0.912	7.87E-11	1.79e-11	33	0.923	0.922	2.54E-11	7.64e-12
34	0.927	0.926	8.87E-11	2.49e-11	34	0.939	0.938	3.8E-11	1.22e-11
35	0.941	0.935	3.33E-10	2.01e-10	35	0.977	0.976	4.19E-10	2.28e-10
44	0.271	0.262	6.99E-10	4.32e-12					
45	0.234	0.231	7.07E-10	3.59e-12	45	0.241	0.232	5.9E-10	5.82e-12
53	0.159	0.158	4.23E-10	4.45e-12	53	0.176	0.174	3.81E-10	1.34e-12
54	0.925	0.925	2.07E-10	1.14e-10	54	0.963	0.963	1.35E-10	1.15e-10
61	0.913	0.918	5.21E-10	1.22e-10	61	0.963	0.963	4.6E-10	1.44e-10
62	0.9	0.9	8.39E-11	1.67e-11	62	0.886	0.886	2.29E-11	4.75e-12
63	0.925	0.925	1.07E-10	3.18e-11	63	0.993	0.993	1.35E-10	6.02e-10
64	0.893	0.889	8.51E-11	1.57e-11	64	0.905	0.902	2.62E-11	6.10e-12
65	0.935	0.933	1.91E-10	1.12e-10	65	0.931	0.931	2.66E-11	8.72e-12
66	0.93	0.9	2.63E-10	1.66e-10					-
67	0.939	0.938	1.57E-10	7.70e-11	67	0.97	0.969	6.2E-11	4.16e-11
68	0.894	0.895	6.75E-11	1.22e-11	68	0.938	0.937	2.92E-11	1.02e-11
69	0.931	0.93	2.23E-10	1.42e-10					-
70	0.929	0.929	2.34E-10	1.49e-10					-
72	0.904	0.921	4.43E-10	1.08e-10	72	0.932	0.942	3.34E-10	7.32e-11
73	0.907	0.905	1.01E-10	2.31e-11	73	0.964	0.963	9.87E-11	6.97e-11
75	0.94	0.938	2.23E-10	1.63e-10	75	0.979	0.964	1.36E-10	2.01e-10
76	0.889	0.888	9.12E-11	1.67e-11	76	0.891	0.891	2.63E-11	5.36e-12
77	0.94	0.94	2.64E-10	1.96e-10	77	0.967	0.982	4.78E-10	1.65e-10
78	0.869	0.869	5.39E-11	8.04e-12	78	0.851	0.851	1.41E-11	3.11e-12
80	0.699	0.723	5.52E-10	2.62e-11	80	0.722	0.74	5.29E-10	1.79e-11
81	0.81	0.817	5.83E-10	4.91e-11	81	0.86	0.866	5.58E-10	4.02e-11
83	0.904	0.902	1.28E-10	3.33e-11	83	0.937	0.936	8.31E-11	3.00e-11
84	0.917	0.917	1.78E-10	7.56e-11	84	0.973	0.96	1.4E-10	1.65e-10

85	0.867	0.866	7.86E-11	1.14e-11	85	0.893	0.893	4.93E-11	8.77e-12
87	0.91	0.91	1.52E-10	4.93e-11	87	0.934	0.933	5.42E-11	1.58e-11
89	0.933	0.934	1.9E-10	1.06e-10	89	0.959	0.946	3.2E-10	1.23e-10
90	0.932	0.933	1.51E-10	6.37e-11	90	0.978	0.972	1.81E-10	2.61e-10
91	0.947	0.932	2.14E-10	1.74e-10	91	0.972	0.969	7.69E-11	5.92e-11
92	0.208	0.206	9.78E-12	2.14e-13	92	0.743	0.737	2.88E-11	2.12e-12
93	0.919	0.922	1.7E-10	6.95e-11	93	0.95	0.95	3.7E-11	1.47e-11
94	0.906	0.902	1.11E-10	2.65e-11	94	0.956	0.955	6.43E-11	2.96e-11
97	0.887	0.89	1.36E-10	3.15e-11	97	0.916	0.916	3.38E-11	8.00e-12
98	0.926	0.925	8.46E-11	2.31e-11	98	0.952	0.951	3.93E-11	1.61e-11
99	0.902	0.901	8.83E-11	1.82e-11	99	0.897	0.896	2.46E-11	5.48e-12
100	0.942	0.94	1.47E-10	7.05e-11	100	0.972	0.969	5.64E-11	3.98e-11
101	0.935	0.948	4.66E-10	1.62e-10	101	0.958	0.959	4.62E-11	2.18e-11
103	0.874	0.873	9.92E-11	1.65e-11	103	0.9	0.899	4.93E-11	9.34e-12
104	0.921	0.92	2.11E-10	1.13e-10					-
105	0.891	0.891	1.92E-10	6.75e-11	105	0.952	0.95	1.39E-10	9.35e-11
111	0.515	0.501	6.22E-10	1.15e-11	111	0.599	0.59	5.14E-10	1.04e-11
112	0.414	0.409	7.06E-10	8.53e-12	112	0.425	0.416	5.73E-10	7.84e-12
115	0.943	0.94	2.41E-10	1.93e-10					-
116	0.864	0.882	6.14E-10	7.17e-11	116	0.897	0.906	5.01E-10	5.07e-11
118	0.956	0.956	2.16E-10	2.09e-10					-
119	0.797	0.786	5.5E-10	4.37e-11	119	0.85	0.843	4.9E-10	3.32e-11
120	0.931	0.931	1.32E-10	4.82e-11	120	0.957	0.957	3.46E-11	1.64e-11
121	0.945	0.945	1.64E-10	9.35e-11	121	0.981	0.98	7.51E-11	8.33e-11
122	0.929	0.929	6.56E-11	1.83e-11					-
123	0.922	0.921	1.61E-10	6.52e-11					-

Table S2.3 Exchange parameters for millisecond dynamics of amide ^{15}N nuclei in PLAAT3 and PLAAT4, assuming a two-state exchange.

PLAAT3				**PLAAT4**			
Residue	**k_{ex} (10^3 s^{-1})**	**p_B (%)**	**$\|\Delta\omega\|$ (ppm)**	**Residues**	**k_{ex} (10^3 s^{-1})**	**pB (%)**	**$\|\Delta\omega\|$ (ppm)**
Global Fit (W24, V50, M51, D56, D81)	1.2(0.3)	n.d	n.d	Dynamic Cluster (R18, L19, Y21, H23, K61, H35)	1.9(0.2)	1.0(0.1)	R18: 2.3(0.3) L19: 1.2(0.1) Y21: 2.6(0.3) H23: 2.0(0.2) H35: 1.2(0.1) K61: 1.3(0.2)

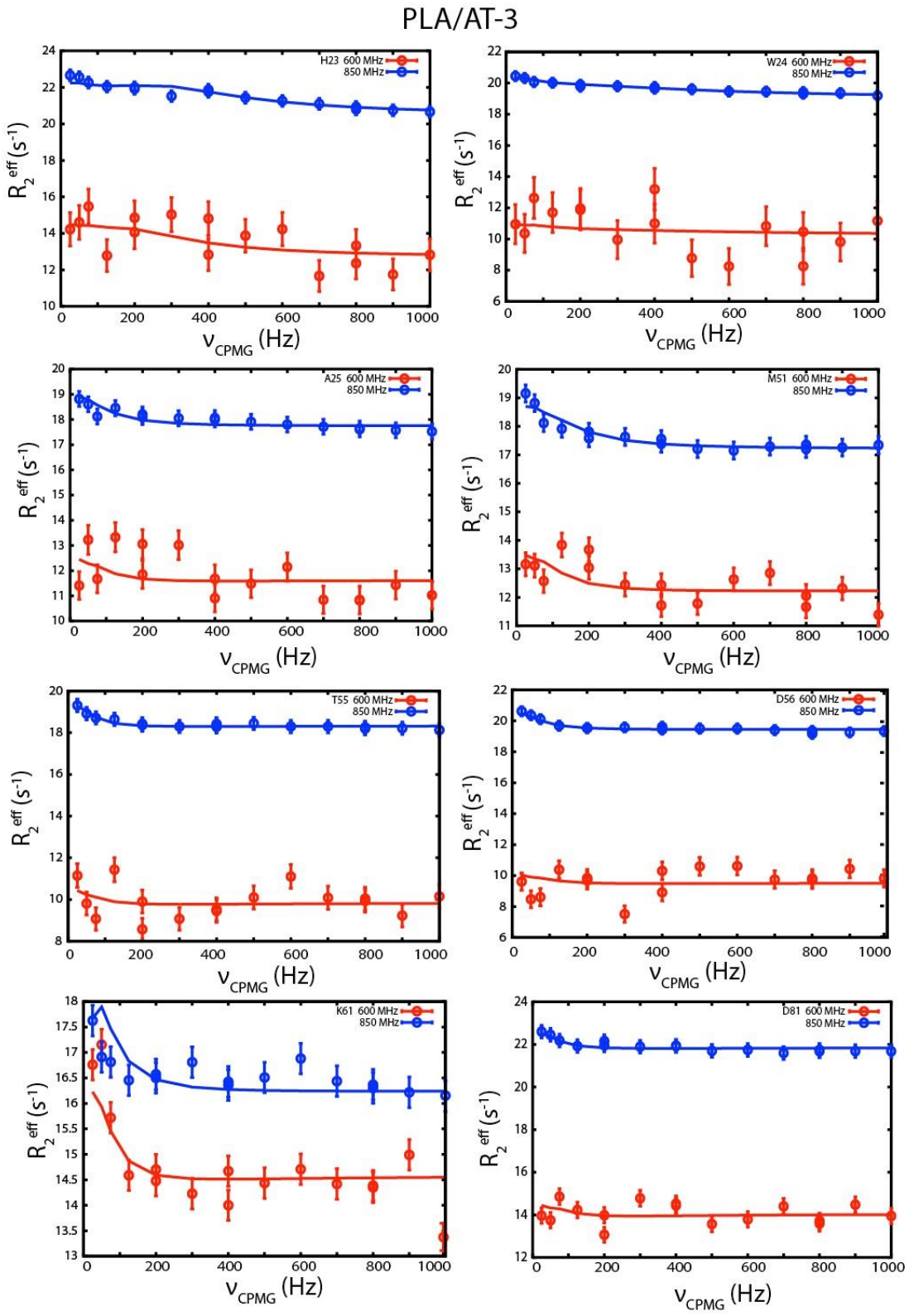

Figure S2.1 Relaxation dispersion curves for PLAAT3. The effective transverse relaxation rates are plotted against the CPMG frequency for the indicated residues. The red and blue curves represent data acquired at 14 T and 20 T, respectively. The experimental data are indicated by circles. The solid lines indicate fits of the combined two-field data to a two-state exchange model.

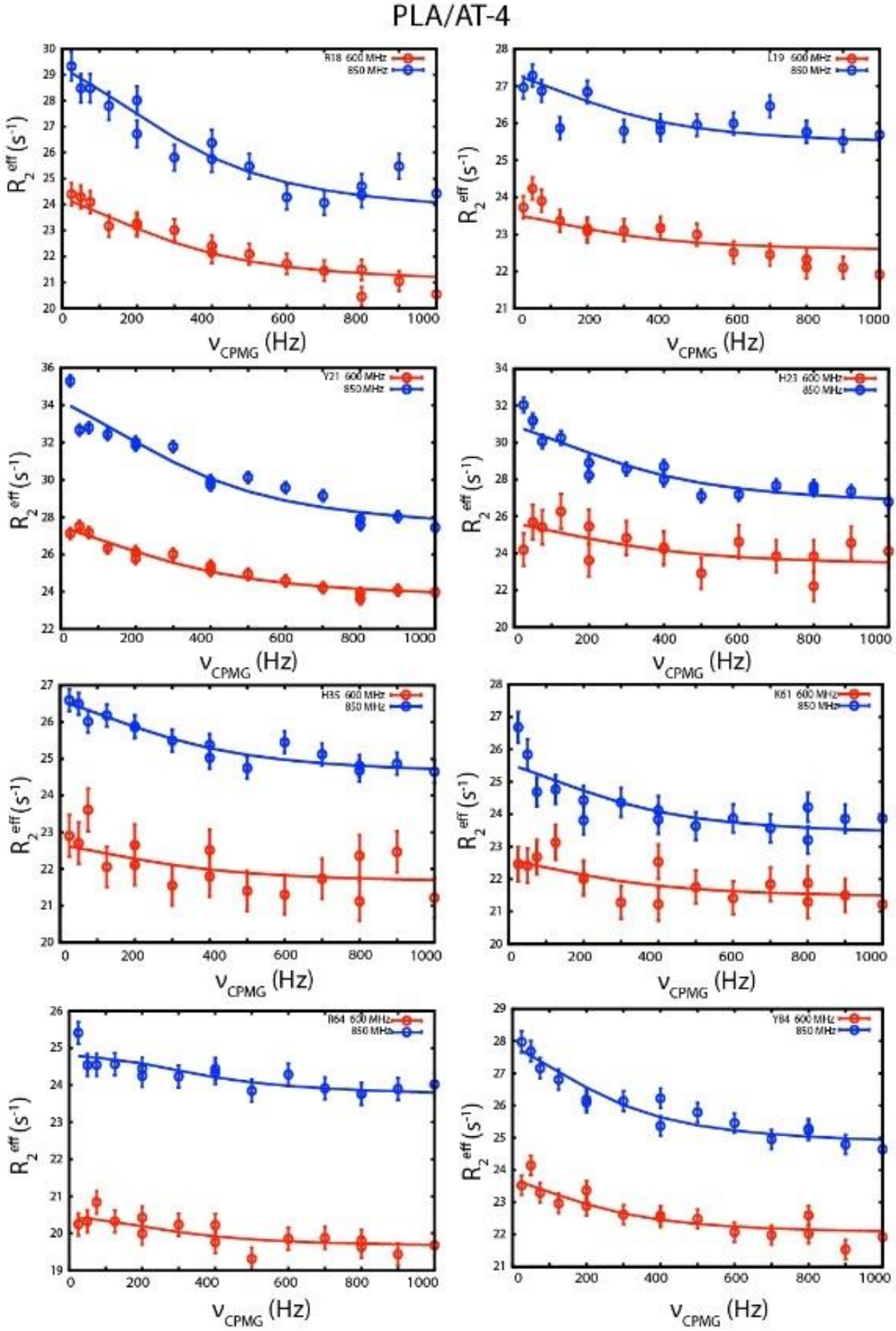
PLA/AT-4
R18 600 MHz
850 MHz
L19 600 MHz
850 MHz
Y21 600 MHz
850 MHz
H23 600 MHz
850 MHz
H35 600 MHz
850 MHz
K61 600 MHz
850 MHz
R64 600 MHz
850 MHz
Y84 600 MHz
850 MHz
R_2^{eff} (s^{-1})
ν_{CPMG} (Hz)

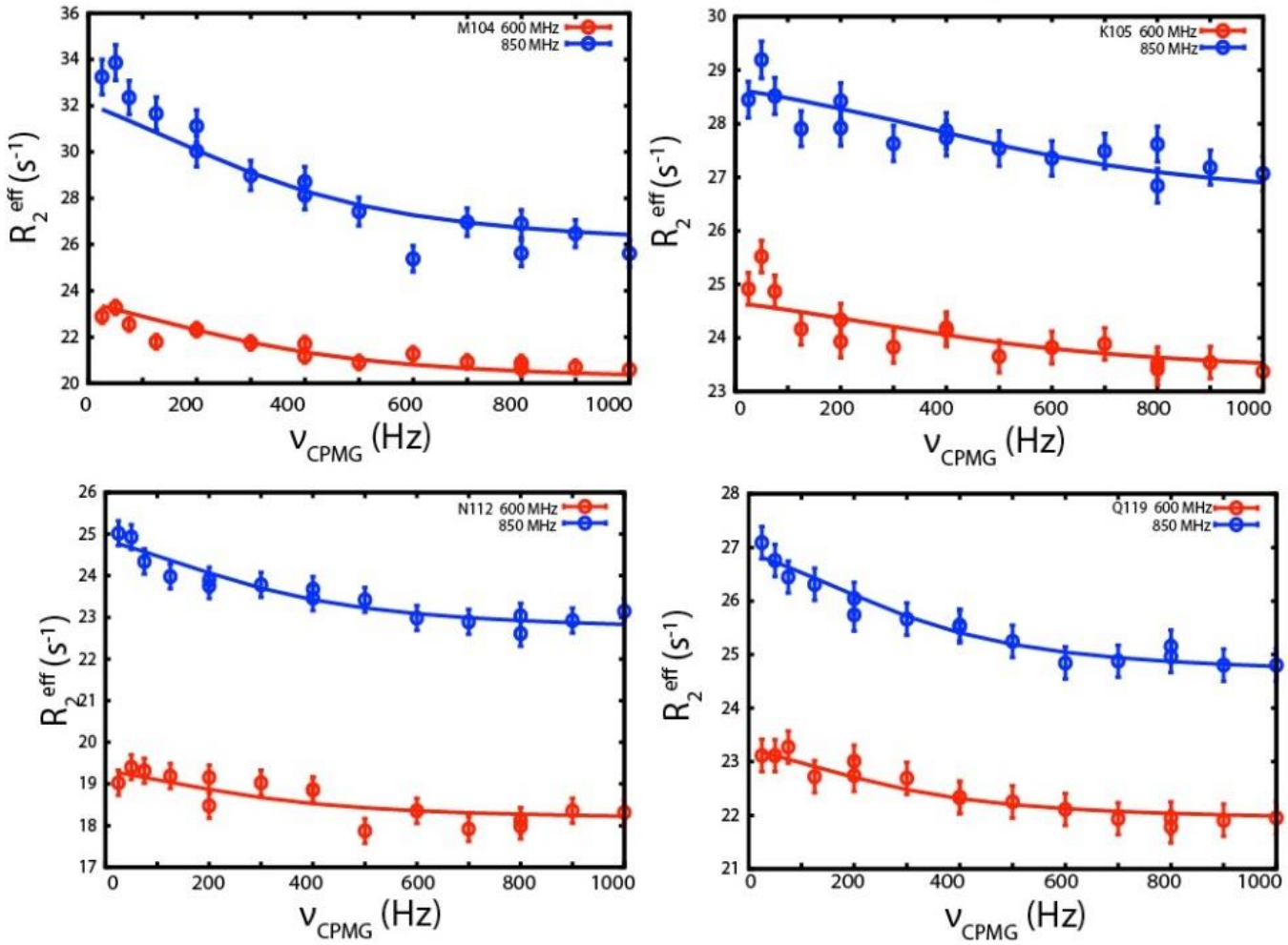

Figure S2.2 Relaxation dispersion curves for PLAAT4. The effective transverse relaxation rates are plotted against the CPMG frequency for the indicated residues. The red and blue curves represent data acquired at 14 T and 20 T, respectively. The experimental data are indicated by circles. The solid lines indicate fits of the combined two-field data to a two-state exchange model.

References

(1) Golczak, M., Kiser, P. D., Sears, A. E., Lodowski, D. T., Blaner, W. S., and Palczewski, K. (2012) Structural basis for the acyltransferase activity of lecithin:retinol acyltransferase-like proteins. *J. Biol. Chem. 287*, 23790–23807.
(2) Anantharaman, V., and Aravind, L. (2003) Evolutionary history, structural features and biochemical diversity of the NlpC/P60 superfamily of enzymes. *Genome Biol. 4*, R11–R11.
(3) Hajnal, A., Klemenz, R., and Schäfer, R. (1994) Subtraction cloning of H-rev107, a gene specifically expressed in H-ras resistant fibroblasts. *Oncogene 9*, 479–490.
(4) Akiyama, H., Hiraki, Y., Noda, M., Shigeno, C., Ito, H., and Nakamura, T. (1999) Molecular cloning and biological activity of a novel Ha-Ras suppressor gene predominantly expressed in skeletal muscle, heart, brain, and bone marrow by differential display using clonal mouse EC cells, ATDC5. *J. Biol. Chem. 274*, 32192–32197.
(5) Shyu, R.-Y., Hsieh, Y.-C., Tsai, F.-M., Wu, C.-C., and Jiang, S.-Y. (2008) Cloning and functional characterization of the HRASLS2 gene. *Amino Acids 35*, 129–137.
(6) Uyama, T., Ikematsu, N., Inoue, M., Shinohara, N., Jin, X.-H., Tsuboi, K., Tonai, T., Tokumura, A., and Ueda, N. (2012) Generation of N-acylphosphatidylethanolamine by members of the phospholipase A/acyltransferase (PLA/AT) family. *J. Biol. Chem. 287*, 31905–31919.
(7) Jin, X.-H., Uyama, T., Wang, J., Okamoto, Y., Tonai, T., and Ueda, N. (2009) cDNA cloning and characterization of human and mouse Ca2+-independent phosphatidylethanolamine N-acyltransferases. *Biochim. Biophys. Acta - Mol. Cell Biol. Lipids 1791*, 32–38.
(8) Husmann, K., Sers, C., Fietze, E., Mincheva, A., Lichter, P., and Schäfer, R. (1998) Transcriptional and translational downregulation of H-REV107, a class II tumour suppressor gene located on human chromosome 11q11-12. *Oncogene 17*, 1305.
(9) Ueda, N., Tsuboi, K., and Uyama, T. (2010) N-acylethanolamine metabolism with special reference to N-acylethanolamine-hydrolyzing acid amidase (NAAA). *Prog. Lipid Res. 49*, 299–315.
(10) Ara, I., Rahman, S., Tsuboi, K., Uyama, T., and Ueda, N. (2014) New players in the fatty acyl ethanolamide metabolism OH OH OH. *Pharmacol. Res. 86*, 1–10.
(11) Ren, X., Lin, J., Jin, C., and Xia, B. (2010) Solution structure of the N-terminal catalytic domain of human H-REV107--a novel circular permutated NlpC/P60 domain. *FEBS Lett. 584*, 4222–4226.
(12) Wei, H., Wang, L., Ren, X., Yu, W., Lin, J., Jin, C., and Xia, B. (2015) Structural and functional characterization of tumor suppressors TIG3 and H-REV107. *FEBS Lett. 589*, 1179–1186.
(13) Uyama, T., Jin, X.-H., Tsuboi, K., Tonai, T., and Ueda, N. (2009) Characterization of the

human tumor suppressors TIG3 and HRASLS2 as phospholipid-metabolizing enzymes. *Biochim. Biophys. Acta - Mol. Cell Biol. Lipids 1791*, 1114–1124.
(14) Pang, X.-Y., Cao, J., Addington, L., Lovell, S., Battaile, K. P., Zhang, N., Rao, J. L. U. M., Dennis, E. A., and Moise, A. R. (2012) Structure/function relationships of adipose phospholipase A2 containing a Cys-His-His catalytic triad. *J. Biol. Chem. 287*, 35260–35274.
(15) Ren, X., Lin, J., Jin, C., and Xia, B. (2010) 1H, 13C and 15N resonance assignments of human H-REV107 N-terminal domain. *Biomol. NMR Assign. 4*, 175–178.
(16) Wang, L., Yu, W., Ren, X., Lin, J., Jin, C., and Xia, B. (2012) 1H, 13C, and 15N resonance assignments of the N-terminal domain of human TIG3. *Biomol. NMR Assign. 6*, 201–203.
(17) de la Torre, J., Huertas, M. L., Carrasco, B., García de la Torre, J., Huertas, M. L., and Carrasco, B. (2000) HYDRONMR: prediction of NMR relaxation of globular proteins from atomic-level structures and hydrodynamic calculations. *J. Magn. Reson. 147*, 138—146.
(18) Lipari, G., and Szabo, A. (1982) Model-free approach to the interpretation of nuclear magnetic resonance relaxation in macromolecules. 1. Theory and range of validity. *J. Am. Chem. Soc. 104*, 4546–4559.
(19) Lipari, G., and Szabo, A. (1982) Model-free approach to the interpretation of nuclear magnetic resonance relaxation in macromolecules. 2. Analysis of experimental results. *J. Am. Chem. Soc. 104*, 4559–4570.
(20) Golczak, M., Sears, A. E., Kiser, P. D., and Palczewski, K. (2015) LRAT-specific domain facilitates Vitamin A metabolism by domain swapping in HRASLS3. *Nat. Chem. Biol. 11*, 26–32.
(21) Palmer, A. (2013) Protein dynamics from NMR spectroscopy and MD simulation. *Biophys. J. 104*, 45a.
(22) Krepl, M., Cléry, A., Blatter, M., Allain, F. H. T., and Sponer, J. (2016) Synergy between NMR measurements and MD simulations of protein/RNA complexes: application to the RRMs, the most common RNA recognition motifs. *Nucleic Acids Res. 44*, 6452–6470.
(23) Trbovic, N., Kim, B., Friesner, R. A., and Palmer 3rd, A. G. (2008) Structural analysis of protein dynamics by MD simulations and NMR spin-relaxation. *Proteins 71*, 684–694.
(24) Zhang, L., Bouguet-Bonnet, S., and Buck, M. (2012) Combining NMR and molecular dynamics studies for insights into the allostery of small GTPase-protein interactions. *Methods Mol. Biol. 796*, 235–259.
(25) Jiang, B., Yu, B., Zhang, X., Liu, M., and Yang, D. (2015) A 15N CPMG relaxation dispersion experiment more resistant to resonance offset and pulse imperfection. *J. Magn. Reson. 257*, 1–7.
(26) Clore, G. M., Szabo, A., Bax, A., Kay, L. E., Driscoll, P. C., and Gronenborn, A. M. (1990) Deviations from the simple two-parameter model-free approach to the interpretation of nitrogen-15

nuclear magnetic relaxation of proteins. *J. Am. Chem. Soc. 112*, 4989–4991.
(27) Orekhov, V. Y., Korzhnev, D. M., Diercks, T., Kessler, H., and Arseniev, A. S. (1999) 1H-15N NMR dynamic study of an isolated α-helical peptide (1–36)- bacteriorhodopsin reveals the equilibrium helix-coil transitions. *J. Biomol. NMR 14*, 345–356.
(28) Fushman, D., Cahill, S., and Cowburn, D. (1997) The main-chain dynamics of the dynamin pleckstrin homology (PH) domain in solution: analysis of 15N relaxation with monomer/dimer equilibration11Edited by P.E.Wright. *J. Mol. Biol. 266*, 173–194.
(29) Korzhnev, D. M., Billeter, M., Arseniev, A. S., and Orekhov, V. Y. (2001) NMR studies of Brownian tumbling and internal motions in proteins. *Prog. Nucl. Magn. Reson. Spectrosc. 38,* 197–266.
(30) Mandel, A. M., Akke, M., and Palmer Arthur G., I. I. I. (1995) Backbone dynamics of Escherichia coli ribonuclease HI: correlations with structure and function in an active enzyme. *J. Mol. Biol. 246*, 144–163.
(31) Altschul, S. F., Madden, T. L., Schäffer, A. A., Zhang, J., Zhang, Z., Miller, W., and Lipman, D. J. (1997) Gapped BLAST and PSI-BLAST: a new generation of protein database search programs. *Nucleic Acids Res. 25,* 3389–3402.